Journal Pre-proof

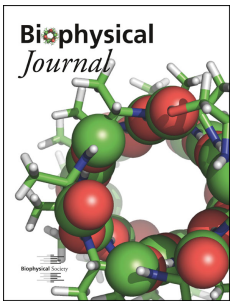

Two separate mechanisms are involved in membrane permeabilization during lipid oxidation

Min Xie, Eveline H.W. Koch, Cornelis A. van Walree, Ana Sobota, Andreas F.P. Sonnen, Eefjan Breukink, J. Antoinette Killian, Joseph H. Lorent

PII: S0006-3495(23)00664-1

DOI: https://doi.org/10.1016/j.bpj.2023.10.028

Reference: BPJ 12623

To appear in: *Biophysical Journal*

Received Date: 29 August 2023

Accepted Date: 25 October 2023

Please cite this article as: Xie M, Koch EHW, van Walree CA, Sobota A, Sonnen AFP, Breukink E, Killian JA, Lorent JH, Two separate mechanisms are involved in membrane permeabilization during lipid oxidation, *Biophysical Journal* (2023), doi: https://doi.org/10.1016/j.bpj.2023.10.028.

Two separate mechanisms are involved in membrane permeabilization during lipid oxidation

Min Xie[a], Eveline H. W. Koch[a], Cornelis A. van Walree[a,b], Ana Sobota[c], Andreas F. P. Sonnen[a,d], Eefjan Breukink[a], J. Antoinette Killian[a] and Joseph H. Lorent[a,e]

[a]Membrane Biochemistry & Biophysics, Bijvoet Center for Biomolecular Research, Department of Chemistry, Utrecht University, Padualaan 8, 3584 CH Utrecht, Netherlands

[b]University College Utrecht, Campusplein 1, 3584 ED Utrecht, Netherlands

[c]Atmospheric Pressure Non-Thermal Plasmas and their Interaction with Targets, Applied Physics Department, Eindhoven University of Technology,

[d]Pathology Department, University Medical Center Utrecht, Heidelberglaan 100, H04.312, Postbus 85500, 3508 GA Utrecht, Netherlands

[e]Cellular and Molecular Pharmacology, Translational Research from Experimental and Clinical Pharmacology to Treatment Optimization, Louvain Drug Research Institute, UCLouvain, Avenue Mounier 73+1, B1.73.05, B-1200 Brussels, Belgium

ABSTRACT

Lipid oxidation is a universal degradative process of cell membrane lipids that is induced by oxidative stress and reactive oxygen and nitrogen species (RONS) in multiple pathophysiological situations. It has been shown that certain oxidized lipids alter membrane properties, leading to a loss of membrane function. Alteration of membrane properties is thought to depend on the initial membrane lipid composition, such as the number of acyl chain unsaturations. However, it is unclear how oxidative damage is related to biophysical properties of membranes. We therefore set out to quantify lipid oxidation through various analytical methods and determine key biophysical membrane parameters using model membranes containing lipids with different degrees of lipid unsaturation. As source for RONS we used cold plasma that is currently developed as treatment for infections and cancer. Our data revealed complex lipid oxidation that can lead to two main permeabilization mechanisms. The first one appears upon direct contact of membranes with RONS and depends on the formation of truncated oxidized phospholipids. These lipids seem to be partly released from the bilayer, implying that they are likely to interact with other membranes and potentially act as signaling molecules. This mechanism is independent of lipid unsaturation, does not rely on large variations in lipid packing and is most probably mediated via short-living RONS. The second mechanism overtakes after longer incubation periods and depends probably on the continued formation of lipid oxygen adducts such as lipid hydroperoxides or ketones. This mechanism depends on lipid unsaturation and involves large variations in lipid packing. This study indicates that polyunsaturated lipids, that are present in mammalian membranes rather than in bacteria, do not sensitize membranes to instant permeabilization by RONS but could promote long term damage.

Statement of significance

Oxidative stress is a common pathophysiological process that leads to the impairment of cell membranes due to the formation of oxidized lipids. Unfortunately, it is unknown how a complex mixture of oxidized lipids impairs membrane function by altering biophysical membrane properties upon lipid unsaturation. We therefore combined analytical techniques to quantify oxidized lipids and correlate their quantity to key biophysical membrane parameters. We observed two mechanisms impairing the integrity of the membrane. One is unsaturation-independent and dominated by truncated lipids, produced by short-living reactive oxygen species. The second is unsaturation-dependent and occurs upon formation of lipid oxygen adducts after longer incubation periods. Both mechanisms trigger the release of oxidized lipids from the membrane, that could constitute signaling molecules.

Abbreviations

CAP, Cold Atmospheric Plasma; **RO(N)S** Reactive Oxygen (and Nitrogen) Species; **LUV**, Large Unilamellar Vesicle; **GUV**, Giant Unilamellar Vesicle; **H_2O_2**, Hydrogen Peroxide; **OH·**, Hydroxyl Radical; **TA,** Terephthalate; **2-HTA**, 2-Hydroxyterephthalate; **Ampliflu™ Red**, N-Acetyl-3,7-dihydroxyphenoxazine; **OxPCs**, oxidized phosphatidylcholine; **HRP**, Horseradish Peroxidase; **HPLC-MS**, High Performance Liquid Chromatography-Mass Spectrometry; **FOX Assay**, Ferrous Oxidation-Xylenol Orange Assay; **AAS**, Atomic Absorption Spectroscopy; **BHT**, Butylhydroxytoluene; **DNPH**, 2,4-Dinitrophenylhydrazine; **DBD-ED**, 4-(N, N-Dimethylaminosulfonyl)-7-(2-aminoethylamino)-2,1,3-benzoxadiazole; **TPP**, Triphenylphosphine; **DPDS**, 2,2'-Dipyridyl disulfide; **DLS**, Dynamic Light Scattering; **GP**, Generalized Polarization; **IPA**, Isopropanol; **LOD**, Limit of Detection; **LOQ**, Limit of Quantification; **PCA**, Principal component analysis.

Introduction

Cell membrane oxidation is a universal degradative process that can ultimately lead to the alteration of membrane properties and cell death. It is usually started by reactive oxygen and nitrogen species (RONS) that induce membrane lipid or protein oxidation in the absence of efficient oxidative defense mechanisms (1). RONS are generated during oxidative stress in pathophysiological situations or as defense mechanism towards infectious germs in phagolysosomes of macrophages and neutrophils to kill invading microorganisms (2, 3). Cold atmospheric plasma (CAP) is a relatively new technology, which mimics this principle to fight bacterial infections or even cancer cells by producing large amounts of RONS *in situ* that can be directly applied to an infected wound or tumor for instance by a plasma pen (4, 5). It has been proposed that the main target of exoplasmically produced RONS is the cell membrane, whose lipids and proteins are subsequently oxidized, leading to alterations of numerous biophysical properties of the membrane that compromise its biological function (6).

In prior studies it has been shown that lipid oxidation and its consequences for biophysical properties of membranes such as permeability or fluidity depend strongly on the lipid composition (1, 7) which is largely organelle- and species-dependent (8, 9). While lipids in membranes of Gram-positive bacteria mainly contain saturated or monounsaturated acyl chains (9) human cell membranes present a much larger distribution of unsaturations, including poly-unsaturated lipids (8). Most phospholipids are asymmetrically unsaturated, containing a saturated and an unsaturated tail at the *sn-1* and *sn-2* position, respectively, while just a minority of phospholipids possesses two saturated or two unsaturated tails (10). Poly-unsaturated lipids are more sensitive to oxidative modifications (11). This is due to the

formation of a pentadienyl radical which is stabilized by the mesomeric effect. Addition of an oxygen molecule to the lipid radical can then produce a hydroperoxyl radical which itself can react with another polyunsaturated lipid, giving rise to another lipid radical and a hydroperoxide. This radical chain reaction is called lipid peroxidation in literature (1).

Several studies showed that the formation of lipid oxides can modulate biophysical properties of membranes and induce pore formation (7, 12, 13). Ytzhak *et al.* found that membranes containing polyunsaturated lipids were more prone to permeabilization. However, they used high concentrations of polyunsaturated lipids such as di-18:2, di-18:3 or di-18:6, which are only found at very small concentrations in cells (7, 10). In a similar experiment on giant unilamellar vesicles (GUV), Bour *et al.* reached no definitive conclusion regarding the presence of lipid unsaturations and sensitivity to permeabilization (14). Usually, the effects on membrane properties and integrity depend on the individual oxidized lipid species that are created. There are strong indications that secondary cleavage products such as lipid aldehydes and carboxylic acids have a stronger effect on permeabilization while lipid hydroperoxides drastically change the area/lipid ratio and induce lipid phase separation but seem to be less effective in permeabilizing membranes (12, 13, 15–17).

While the effects of single oxidized lipid species on certain biophysical properties have become apparent, it is not clear how a complex combination of oxidized lipids, which is biologically more relevant, would induce changes to membrane properties. This is mainly due to the difficulty to simultaneously quantify each oxidized lipid species. A comparison on how symmetric e.g. PC(18:1/18:1) versus asymmetric e.g. PC(16:0/18:1) monounsaturated or polyunsaturated lipids (**Fig. 1B**) sensitize membranes to oxidative damage is also lacking. Further, the distinction between direct damage to membranes by RONS versus long-term effects from continuous reactions such as lipid peroxidation after post-incubation periods is often omitted. This is biologically highly relevant since an initial small-scale damage could eventually develop into serious membrane alterations in the absence of efficient antioxidant repair mechanisms. In this perspective, we investigate short- and long-term permeabilization and membrane packing in parallel to molecular changes induced by RONS that are produced *in situ* by cold atmospheric plasma in large unilamellar vesicles (LUVs) composed of symmetrical and asymmetrical mono- and polyunsaturated lipids. To determine the enounced properties, we use a combination of biophysical, biochemical and analytical approaches described hereunder.

Results

RONS production by KINPen IND®

To produce RONS, we used the KINPen® which is a plasma pen that has been optimized to produce a large amount of hydroxyl radicals (18). In our setup (**Fig. 1A**), the generated plasma plume does not touch the liquid suspension which contains the membrane models - large unilamellar vesicles (LUVs). The electric field will not interfere in vesicle permeation because it is too weak outside the plume, meaning that permeabilization or other changes of membrane properties will be induced by lipid oxidation. We first assessed the quantity of RONS that were produced in our setup by determining the amount of hydroxyl radicals (OH•) and hydrogen peroxide (H_2O_2) at the corresponding incubation times

(**Fig. S1A, B**). While hydroxyl radicals were detected at micromolar range, H_2O_2 reached millimolar levels at 20 min CAP treatment. Since the quantity of RONS that is produced in the chosen condition is reproducible, we assume that main differences on membrane effects resulted from initial lipid compositions.

Permeabilization by RONS is mediated via two different mechanisms

Potassium ions (K^+) play important roles in many cellular processes (19), especially in membrane potential maintenance. The lipid bilayer of cell membranes is generally not permeable towards K^+, with the concentration gradient between the cytoplasm and exoplasm being mainly maintained by the Na^+/K^+-ATPase pump. Here we quantified K^+ leakage in LUVs made of phosphatidylcholine lipids with different symmetric or asymmetric combinations of mono- and polyunsaturated acyl chains by atomic absorption spectroscopy (AAS) directly upon CAP treatment and after a 20 h post-incubation period at ambient temperature.

We started out with several control experiments to rule out factors that could potentially influence membrane permeability or lipid oxidation. First, a difference in osmotic pressure between the inside and the outside of vesicles may favor permeabilization of LUVs. Since CAP induces the formation of new species, we might observe a significant increase of osmolarity outside of vesicles. However, during all our setups, no significant change of osmolarity could be observed during treatment, ruling out this possibility (**Fig. S2A**). As described earlier, also the effect of the generated electric field and hence electro permeabilization can be ruled out in our current setup. Furthermore, acidity is an important factor which could influence lipid oxidation. However, the pH remained unaffected in our setup, excluding related effects (**Fig. S2B**).

As shown in **Fig. 2A**, CAP induced a gradual K^+ release from LUVs during a 10-40 min treatment period. The rate of K^+ release (***k***-value) in these four different LUVs compositions does not appear to vary significantly during the 10-40 min treatment period, indicating that unsaturations do not sensitize membranes towards direct RONS damage (**Fig. 2C**). By contrast, after a 20 h post-CAP treatment period, the amount of K^+ release increased particularly in poly-unsaturated PC lipids i.e. PC(16:0/18:2) and PC(18:2/18:2) (**Fig. 2B**) with the ***k***-value related to the rate of release increasing only in LUVs made of polyunsaturated lipids (**Fig. 2C**). These results indicate two different release mechanisms, one independent of unsaturation and another depending strongly on unsaturation. Curiously, we observed that K^+-release was always higher in PC(16:0/18:1) LUVs than in PC(18:1/18:1) LUVs, suggesting that oxidized lipid species of asymetrically monounsaturated lipids might be more powerful in permeabilizing the membrane.

Membrane packing alterations by RONS depend on lipid unsaturations

Packing of lipid membranes is an important biophysical property which is related to many functional aspects of membranes, such as permeability and lateral diffusion of lipids and proteins. Modulation of membrane packing through external or internal stimuli can have large consequences for the evoked functions and can lead to the impairment of membrane signaling and cell death in absence of adaptation (20, 21). To examine if CAP alters membrane packing, we applied two environmental polarity sensitive

dyes, Laurdan and di-4-ANEPPDHQ, which have been widely used to quantify membrane packing in both model membranes and living cells (22, 23). In principle, di-4-ANEPPDHQ probes only the outer leaflet of the membrane bilayer due to its positive charges and hence incapacity to flip to the inner leaflet (24). If damage occurs only to the outer leaflet, this probe should be more sensitive than Laurdan. Further, the fluorophore of di-4-ANEPPDHQ is assumed to probe polarity close to the headgroup/water interface (25). Laurdan probes the polarity of both membrane bilayer leaflets in between acyl chains and lipid headgroups (26, 27), hence at a slightly deeper location in the membrane bilayer than di-4-ANEPPDHQ.

We observed that oxidation induced a slight increase of Laurdan Generalized Polarization (GP) in all LUVs after 40 min of CAP treatment, indicating either that less water molecules are in the vicinity of Laurdan and packing has increased, or the polarity of its microenvironment has decreased (**Fig. 3A**). After 20 h of post-incubation, we observed a large increase of Laurdan GP only in polyunsaturated lipids (**Fig. 3A**), similar to the strong increase of permeabilization (**Fig. 2B**). Changes of similar magnitude appeared measuring di-4-ANEPPDHQ GP, but surprisingly into the opposite direction, with a decrease of GP, indicating less packing or an increase of the polarity in the microenvironment (**Fig. 3B**). These opposite trends could arise from the fact that CAP induces differential changes upon membrane depth which might be explained by the large variety of oxidized species being formed (see below). A somehow compensatory effect might also explain the absence of large packing changes probed by di-4-ANEPPDHQ on PC(16:0/18:2) after post-incubation.

Quantification of oxidized phosphatidylcholines (OxPCs)

Production and diversity of hydroperoxides

To examine the complex relationship of permeabilization or membrane packing with the formation of oxidized phosphatidylcholines (OxPCs), we quantified and characterized the formation of OxPCs upon incubation of LUVs with RONS, generated by CAP. For the quantification of total hydroperoxides in LUVs, the FOX assay was used (**Fig. 4A**) (28–30). In PC(16:0/18:2) and PC(18:2/18:2) LUVs, lipid hydroperoxides were further quantified by HPLC-UV-MS, taking advantage of the specific UV absorbance of conjugated dienes at 234 nm (**Fig. S3**). A comparison of both methods revealed an equal specificity towards hydroperoxides albeit that the FOX assay gives higher values because it determines the amount of all -OOH functions in the lipid extract while the LC-UV method determines the amount of individual -OOH lipids. We observed that RONS produced by CAP induced detectable amounts of lipid hydroperoxides only in LUVs made of poly-unsaturated lipids, e.g. PC(16:0/18:2) and PC(18:2/18:2) (**Fig. 4A, Fig. S3**). Twenty hours post-incubation led to a huge increase of hydroperoxides in these LUVs, especially in PC(18:2/18:2), indicating a strong dependence on the number of unsaturations.

The distribution of hydroperoxide species in PC(16:0/18:2) and PC(18:2/18:2) LUVs is summarized in **Fig. 5A**, B. The complexity and diversity of lipid hydroperoxides rose upon increasing numbers of unsaturated double bonds (**Fig. 5A**, B, **Fig. S3**). Hydroperoxides with one -OOH were the most abundant in both PC(16:0/18:2) and PC(18:2/18:2) LUVs, followed by those with two -OOH or three -OOH functional groups.

Production and diversity of OxPCs with truncated acyl chains

Next, we focused on lipid oxides with truncated acyl chains, including lipid aldehydes and carboxylic acids that can be produced from the decomposition of lipid hydroperoxides at the unsaturation sites via Hock rearrangement or the formation of a dioxetane (31, 32). DNPH derivatization in combination with LC-MS-UV was used to quantify truncated and non-truncated aldehydes and ketones (33). Truncated phospholipids with aldehyde and ketone groups were by far the most common products while ketone addition products were only obtained in significant amounts in polyunsaturated lipids (~10 % in PC (16:0/18:2) and 10-20 % in PC (18:2/18:2) out of their corresponding total DNPH signal) (**Fig. 5E**, **F**). In PC (18:2/18:2), a small amount of DNPH peak area (5-10%) after 20h of post-incubation contained truncated lipids and addition products, which made it impossible to assign this quantity to any of the products (**Fig. 5F**). Interestingly, we observed that the total amount of aldehydes and ketones was similar in lipids with symetrically unsaturated acyl chains (PC(18:1/18:1) and PC(18:2/18:2)) and significantly higher compared to asymmetrically unsaturated acyl chains PC(16:0/18:1) and PC(16:0/18:2)) directly after CAP treatment (**Fig. 1** and **Fig. 4B**). This implies that production of these species depends on the number of unsaturated acyl chains, rather than the total number of lipid unsaturations. Noticeably, 20 h post-incubation only resulted in further accumulation of these species in PC(18:2/18:2) LUVs, and this seemed mainly due to the accumulation of ketone addition products.

Conversely to the amount of lipid aldehydes, the diversity of aldehyde species increased upon the total number of unsaturations. The variety of species is summarized in supplementary tables (**Supplementary file**, **S3, S4, S5, S6**).

In addition to aldehydes, lipid carboxylic acids constitute the most common truncated OxPCs. Lipid carboxylic acids derive from either the oxidation of lipid aldehydes or the decomposition of secondary oxidized products, e.g. lipid hydroperoxides, ketones, hydroxides and ozonides (34). The total amount of lipid carboxylic acids seemed to be positively correlated with the total number of unsaturated double bonds and post-incubation induced only slight changes (**Fig. 4C**).

Production and diversity of other OxPCs

Lipid hydroxyls, ketones or epoxides can be formed by either rearrangement of lipid hydroperoxides or direct formation by reacting with hydroxyl radicals (35, 36). Moreover, ozone (O_3), that is also produced by CAP, reacts with unsaturated lipids as well, resulting in ozonides (37, 38). Considering the lack of standardized quantitative approaches for the determination of these oxidized lipid species (except ketones, **Fig. 5C, D, E, F**), and their relatively small amount, we applied a semi quantitative approach (39) by presenting the distribution of OxPCs with different numbers of oxygen atoms in **Fig. S4**. We observed that more oxygen atoms were added to host lipids upon CAP treatment time and post-incubation, and that this trend also depended on unsaturations, i.e. poly-unsaturated LUVs have ~10 times more addition of oxygen than mono-unsaturated LUVs. We further observed that the largest relative peak area could be related to the formation of hydroperoxides especially in polyunsaturated lipids (**Fig. S4, *OO**).

OxPCs are released from host LUV bilayer

To investigate whether OxPCs remain in the membrane of host LUVs, or whether they escape the membrane and adsorb at the air-water interface, we measured the surface tension after various treatment conditions. In this "pendant-drop" experiment, a drop is formed instantly, and directly hereafter amphiphilic substances can adsorb at the air-water interface upon the time scale of the experiment (**Fig. 6**). A reduction in surface tension is hence induced by the adsorption of amphiphilic molecules e.g. surfactants, at the water-air interface. For LUV controls without CAP treatment (**Fig. 6A**), no significant decrease in surface tension was observed within the observation time scale, regardless the number of unsaturations, meaning there was no release of phospholipids into the air-water interface on the time scale of the experiment. Triton X-100, a known surfactant, effectively reduced surface tension in buffer (**Fig. S5A**) and LUV suspensions (**Fig. 6A**), showing its potency in adsorbing at the water-air interface.

CAP treatment reduced surface tension in all LUV suspensions (**Fig. 6A**) but not of pure PBS buffer, indicating that RONS on their own have no effect on surface tension reduction, but oxidized lipids do (**Fig. S5B**). Post-incubation caused a slightly larger reduction of this interfacial tension only in LUVs made of PC(18:2/18:2). Our results indicate that certain OxPCs are released from the host LUV membrane bilayer and adsorb at the air-water interface, thereby reducing surface tension (**Fig. 6B**) (40, 41).

Interestingly, DLS analysis shows neither a significant reduction in average size for all treated LUVs nor the formation of small aggregates such as micelles (**Fig. S6A**, **B**, **C**, **D**). This could mean that only a small amount of the formed OxPCs is released from the host LUV membrane bilayer into the aqueous phase, the air-water interface. Another possibility is that the reduction of size of LUVs due to the release of certain oxidized lipids is compensated by the formation of molecules with a larger molecular surface than the original phospholipids such as lipid hydroperoxides (17).

Lipid oxidation increases the polarity of lipids especially if oxidation leads to truncation of an acyl chain such as during the formation of aldehydes or carboxylic acids (**Table S1**). According to the prediction of logP (**Table S1**), the effective partitioning into the aqueous phase should increase by a factor of ~10^2 if an oxygen atom is added to the acyl chains, and by a factor of ~10^5 if the chain is oxidatively truncated. The chances are hence large that truncated phospholipids can effectively partition into the aqueous phase.

Interestingly, the rate by which the surface tension is decreased depends strongly on the structure of the oxidized lipid (**Fig. S5B**) and is different for post-incubation in PC(18:2/18:2) (**Fig. 6A**). The residence time of a lipid in a bilayer is commonly defined as $\tau_R = \tau_0/e^{-\Delta E/kT}$ where τ_R is the mean residence time in s^{-1}, τ_0 is the motional correlation time for amphiphiles in bilayers (~10^{-7} s), ΔE is the activation energy for the lipid to escape the bilayer, *k* is the Boltzmann constant and *T* the temperature in Kelvin. This expression can be approximated by $\tau_R \approx 55\tau_0/CMC$, where CMC is the critical micellar concentration of the lipid (or critical aggregation concentration for bilayer forming lipids). From the measured CMC/CAC of phospholipids, the escape rate should increase by a factor of 4-10 if 2 CH_2 groups are "cut-off" the lipid (42, 43). From these theoretical considerations, it seems that truncated lipids are the best candidates to be quickliest released from the bilayer and hence reduce surface tension.

Principal component analysis (PCA) of membrane properties and lipid oxidation

A PCA reveals the connection of different parameters in treated samples by visualizing variations of multiple parameters into a two-dimensional space. In our analysis, the directions of brown arrows indicate the development of parameters such as permeability etc. (**Fig. 7**). If arrows are almost parallel, parameters are positively correlated and evolve into similar directions (increase or decrease) upon samples (LUVs) and conditions (control, CAP treatment, post-incubation). If the arrows point into opposite directions, the parameters are negatively correlated, meaning if one parameter increases, the other decreases or vice-versa. Conversely, if arrows are perpendicular, then these parameters are probably not correlated. LUV samples that are close on the PCA coordinate system have similar properties.

The most informative PCAs were obtained comparing control samples vs. 40 min treated CAP samples without post-incubation (**Fig. 7A**), and 40 min CAP treatment without post-incubation vs. 40 min CAP treatment with 20 h post-incubation (**Fig. 7B**).

PCA revealed that all LUV samples evolved into similar directions on the PCA plane upon direct CAP treatment, meaning that oxidation of lipids, permeabilization, packing developed similarly for all samples, regardless of lipid unsaturations (**Fig. 7A,** green and purple arrows). We observed further that permeabilization was closely linked to the formation of truncated aldehydes and ketones, slightly less to carboxylic acids, while hydroperoxides and ketone adducts seemed less correlated to this trend (**Fig. 7A,** brown arrows). This means that hydroperoxides and ketone adducts play a minor role in the permeabilization mechanisms for direct treatment, which is supported by the fact that no hydroperoxide and almost no ketone adduct is formed for monounsaturated lipids although permeabilization is progressing (**Fig. 2A, Fig. 4A, Fig. 5C, D**)**.** Interestingly, surface tension evolved into the opposite direction of especially truncated aldehydes and ketones, and carboxylic acids, meaning that surface tension decreased upon formation of especially truncated oxidized phospholipids (**Fig. 7A**).

Comparison of samples treated for 40 minutes and that were either submitted to 20 h post-incubation or not provided a different picture. Sample points of polyunsaturated lipids (purple arrows) evolved strongly on the PCA plane (large distances) while differences for monounsaturated lipids remained small (green arrows) (**Fig. 7B**). This means that post-incubation affects mainly LUVs of polyunsaturated lipids. Changes to permeabilization, due solely to post-incubation, were less linked to the formation of truncated lipids but rather to hydroperoxide and ketone adducts formation (**Fig. 7B,** brown arrows). It appears though that long-term permeabilization might be promoted by oxygen addition products such as hydroperoxides. This implies that permeabilization proceeds possibly via two different mechanisms. One that is quite rapid and depends on acyl chain breaking, and another that depends on longer post-incubation periods and the formation of oxygen addition products. Surface tension was here also rather linked to the formation of hydroperoxides and ketone adducts, meaning that their release to the aqueous environment or the air-water interface is slower, as discussed before (**Fig. 7A**, **B**).

The picture for packing investigated by di-4-ANEPPDHQ and Laurdan GP is less clear, although large changes in GP appear only upon the formation of oxygen addition products (**Fig. 3A**, B and **Fig. 7B**).

It is unfortunately not sure how other lipid oxides such as hydroxyls, epoxides or ozonides might contribute to changes of membrane properties since we did not quantify them in an absolute manner (**Fig. S4**). However, the relative increase of these peaks in LC-MS is very small compared to the formation of truncated oxidized phospholipids or ketones addition products plus hydroperoxides, especially in polyunsaturated lipids (**Fig. S4**), suggesting that the quantified oxidized lipids should be responsible for the main effects observed.

Discussion

Lipid peroxidation is ubiquitous but the modulation of different biophysical properties of the membrane upon formation of oxidized lipids is still poorly understood because of the huge complexity of possible oxidation products in biological and even model membranes. By using model membranes made of mono- and poly-unsaturated lipids with one unsaturated (asymmetric) or two unsaturated (symmetric) acyl chains, we analyzed how structural properties of lipids guide the alteration process of membranes upon oxidation and identified the main oxidized lipid species that are responsible.

Our data, combined with PCA suggests that two different permeabilization mechanisms exist. The first mechanism leads to rapid permeabilization in parallel to the formation of truncated lipids, in mono and polyunsaturated lipids. Hence, the associated oxidative cleavage does not depend on the unsaturation degree, if at least one unsaturation is present. The formation of cleaved lipid aldehydes and carboxylic acids can happen via formation of hydroperoxide intermediates and subsequent Hock cleavage or dioxetane formation (44). This mechanism is based on hydrogen abstraction from the C_α carbon of the acyl chain. Another mechanism to produce truncated lipids is based on the formation of Criegee ozonides which requires the formation of ozone, produced by the CAP source (45, 46). Since there are almost no hydroperoxides present in the mono-unsaturated models, oxidative cleavage might not rely on the intermediate of hydroperoxides here – except if they are very unstable in the present conditions. The kINPen produces a cold plasma containing a large variety of RONS, thus it is difficult to say which oxidation mechanism is dominating. We can assume that short-living reactive species (OH•, OOH•, O, O_3, O^{2-}., $^1O_2$) play a major role here since they can induce fast hydrogen abstraction and subsequent acyl chain truncation. The kINPen is known to generate large amounts of hydroxyl radicals, as it has been determined in **Figure S1**, thus these might be the main species inducing short-term damages (47). It has earlier been shown that indirect treatment by plasma does not induce direct permeabilization, excluding a significant effect of long-living RONS (48).

It has been proposed in other studies that truncated lipids are the driving factor for membrane permeabilization (12, 13, 49–51). Generally, an increase of positive intrinsic molecular curvature due to truncation of the acyl chains goes along with an increase of polarity of the side chain due to aldehyde or carboxylic acid formation (**Table S1**). This parallel increase of membrane polarity and the amount of positively curved lipids could lead to the formation of toroidal pores at a certain threshold of oxidized lipids (13, 52). The truncated lipids, or their short chain oxidized counterparts, are probably also responsible for the observed reduction of surface tension as discussed before. Since there is no

363 decrease of LUV size, chances are real that the amount of released lipids is small, especially since no
364 hydroperoxides with a high molecular surface area are formed in LUVs of monounsaturated lipids that
365 could compensate for the area change.

366 The continuous K+ release observed during this “fast” mechanism could be explained by a) the
367 formation of short living “membrane instabilities” that are associated with the instant formation of
368 truncated lipids by short living RONS, b) formation of toroidal pores which are only formed at a certain
369 threshold concentration of truncated lipids and which is inhibited by the constant release of pore forming
370 OxPCs from the membrane or c) the asymmetric oxidation of both monolayers. In our case, the
371 formation of truncated lipids in the outer monolayer could create a concentration gradient, forcing the
372 flipping of these oxidized lipids to the inner leaflet and thereby creating possible transient instabilities.
373 Preferential oxidation of the outer monolayer has been proposed as a mechanism in GUV membrane
374 destabilization (51).

375 The second permeabilization mechanism is only observed during long-term incubation of
376 polyunsaturated lipids. Since only hydroperoxides increased strongly in LUVs with polyunsaturated
377 lipids upon post-incubation, we suspect that this “slow” permeabilization is based on hydroperoxide
378 formation, even though other addition products such as ketones might play a role. Interestingly, this
379 permeabilization is coupled to a huge increase in Laurdan GP. This increase in packing or reduction of
380 the water incursion might be due to the increase in surface area per molecule which is predicted upon
381 formation of hydroperoxides. Formation of hydroperoxides might also induce a lateral rearrangement
382 of other oxidized lipids in the membrane. It has been shown that hydroperoxides are able to phase
383 separate from other lipids (17, 53), meaning that the effective surface for other oxidized lipids such as
384 aldehydes or carboxylic acids on a LUV could be reduced, which would increase their local
385 concentration and hence their efficiency in permeabilizing membranes. If hydroperoxides are mainly
386 created on the outer monolayer, the area increase of the outer monolayer could create an area
387 difference between inner and outer leaflet and thereby promote membrane instabilities (51). Effects
388 related to area difference should in theory be compensated by quickly flip-flopping lipids such as
389 cholesterol, which is not present in our models.

390 A threshold for permeabilization by oxidized lipids was proposed by several authors (12, 54). Runas *et*
391 *al.* observed a large increase of passive diffusion of an uncharged molecule from 2.5-10 % POxnoPC
392 i.e. PC(16:0/9:0<CHO@C9>). At this concentration of oxidized lipid, no diffusion of charged molecules
393 through the membrane was observed. Above 12.5 %, charged dextran of a size of 54.5 nm was able to
394 cross the membrane, implying the formation of pores that exceeded this size (54). Since we observe
395 the permeation towards the small but charged potassium ion, these thresholds might be different - if
396 they even exist. After 10 min of treatment, we observe 10-20 % of total potassium release associated
397 with 5-8 % of lipid aldehydes or 0.5-5 % of carboxylic acid formation. It is not clear how the association
398 of a variety of different aldehydes and carboxylic acids might play a role in permeabilization.

399 Laurdan and di-4-ANEPPDHQ GP were altered differently upon oxidation. This difference might either
400 arise from different locations of the probes in the membrane z-axis (55), from the fact that di-4-
401 ANEPPDHQ is leaflet selective and hence might only probe the outer leaflet if there is no flipping (24),
402 or from the fact that both molecules probe different properties (56). The PCA analysis revealed that
403 both probes develop into different directions upon oxidation but also upon the number of lipid

unsaturations in the controls. Packing was further no indication of potassium release except maybe during the formation of hydroperoxides upon post-incubation. The largest changes in GP were observed only for conditions with post-incubation, and only in membranes containing polyunsaturated lipids. This implies that certain oxygen addition products strongly alter packing, or the polarity in the vicinity of the fluorophores. Hydroperoxides are supposed to point their hydrophilic peroxyl group to the membrane interphase which could alter polarity and packing in the vicinity of the probes (17). The observed changes merit further attention since the use of these probes in more complex membranes might be useful to detect the formation of specific oxidation products.

The release of oxidized lipids from the membrane could have potential impacts *in vivo* for multiple organisms. During situations of oxidative stress in humans, OxPCs could act as signaling molecules for other distant cells similar to cytokines such as prostaglandins, which are derived from arachidonic acid. This might especially be true for hydroperoxides that have shown to induce processes such as ferroptosis (57).

Our observations provide useful insights on how RONS interact directly with cell membranes. This information is especially useful to predict effects on phagocytosed microorganisms which are subjected to large amounts of RONS produced during the oxidative burst. Since already small amounts of oxidized lipids seem to have an effect on membrane permeability, and especially toward ions which usually maintain the membrane potential, it is foreseeable that ATP production through F-ATPases is compromised because it predominantly relies on the membrane potential component of the proton motive force (58). Lipid oxidation might thus be a very effective way on compromising microorganisms. This principle is used by CAP which is undergoing many clinical trials on its effectivity on bacterial infections (59–61). CAP is further used in clinical trials for especially head and neck cancers (62, 63). Lipid oxidation could here also play an important role, not only in changing biophysical properties of the membrane but also in producing “signaling” lipid oxides as discussed before.

All in all, we concluded that there exist probably at least two permeabilization mechanisms in oxidized membranes and that these mechanisms have different dependencies regarding lipid unsaturations, acyl chain asymmetry and incubation periods.

Materials and methods

Chemicals and reagents

Argon (purity 5.0) was ordered from Linde plc (IRE). 1-palmitoyl-2-oleoyl-glycero-3-phosphocholine (POPC, PC(16:0/18:1), 1,2-dioleoyl-*sn*-glycero-3-phosphocholine (DOPC, PC(18:1/18:1), 1-palmitoyl-2-linoleoyl-sn-glycero-3-phosphocholine (PLPC, PC(16:0/18:2), 1,2-dilinoleoyl-sn-glycero-3-phosphocholine (DLPC, PC(18:2/18:2), 1-palmitoyl-2-(9'-oxo-nonanoyl)-sn-glycero-3-phosphocholine (PC(16:0/9:0<CHO@C9>)@C9, ALDO PC) and 1-palmitoyl-2-azelaoyl-sn-glycero-3-phosphocholine (PC(16:0/9:0<COOH@C9>), PAze PC) were purchased from Avanti Polar Lipids (USA). Sodium terephthalate (TA), 2-hydroxyterephthalate (2-HTA) and 4-(*N*,*N*-Dimethylaminosulfonyl)-7-(2-aminoethylamino)-2,1,3-benzoxadiazole (DBD-ED) were obtained from TCI EUROPE N.V. (NL). 13(*S*)-Hydroperoxyoctadeca-9Z,11E-dienoic acid (13-HPODE) was purchased from Cayman Chemical. 2,4-

Dinitrophenylhydrazine (DNPH, ⩾98%) was ordered from Acros Organics (NL). Di-4-ANEPPDHQ was ordered from Thermo Fisher Scientific Inc. Triphenylphosphine (TPP), 1-(6-(dimethylamino) naphthalen-2-yl) dodecan-1-one (Laurdan), Xylenol Orange tetrasodium salt, Ampliflu™ Red (10-Acetyl-3,7-dihydroxyphenoxazine), horseradish peroxidase, Valeraldehyde-2,4-DNPH and 2,2'-dipyridyl disulfide (DPDS) were all ordered from Merck (USA). For all preparations, ultrapure water (Milli-Q-H_2O) is used at 18.2 MΩ.cm.

Plasma source

For our experiments, we used the kINPen® IND plasma pen as RONS source (**Fig. 1A**). Inside the plasma jet a high electric voltage (2-3 kV) is generated by a high frequency generator (1 MHz) connected to a steel electrode inside a ceramic capillary (47). The vector gas argon flows through the capillary and the high frequency discharge converts the vector gas into a cold plasma. Argon was used at a flow rate of 4.2 standard liters per minute (slm) and the plasma source operated in the burst mode which adds a square kHz wave (on-off) on top of the MHz frequency to reduce the production of heat, keeping the plasma at a temperature of ~40 ºC. To provide stable and reproducible plasma treatments, the plasma source was switched on at least 20 minutes before treatment. The treated sample was at a 20º angle to induce constant agitation of the liposome suspension caused by the high vector gas flow. Therefore, the plasma plume generated was not in direct contact with the liposome suspension (**Fig. 1A**).

Quantification of OH• radical and H_2O_2 produced from CAP

Production of OH• radical was quantified with terephthalate (TA) that is transformed into 2-hydroxyterephthalate (2-HTA) upon reaction with hydroxyl radicals (64). Specifically, 4 mM of TA was added in 1 ml of PBS buffer in glass beaker, and it was placed under plasma plume as indicated in Fig. 1a. After treatment, certain amount of Milli-Q-H_2O was added back to compensate water loss during the treatment. 2-HTA was used to make a calibration curve which concentration ranged from 0 to 100 µM. Excitation and emission wavelength at 310 nm and 430 nm, respectively, were used to determine the fluorescence of 2-HTA (CLARIOstar reader, BMG LABTECH).

Production of H_2O_2 from CAP was determined with Ampliflu™ Red (64). Specifically, 1 ml of PBS buffer was treated with CAP for different time first, and afterwards, 2 µM of Ampliflu™ Red and 0.1 U/ml of horseradish peroxidase (HRP) were added into the treated PBS. Commercial H_2O_2 (Honnywell, 30 % (w/w) in H_2O) was used to make the calibration curve. The incubation was kept at room temperature for 20 minutes. Excitation and emission wavelength at 563 nm and 587 nm were used to determine the fluorescence of resorufin (oxidized product of Ampliflu™ Red by H_2O_2) CLARIOstar reader (BMG LABTECH). Quantities of RONS described in this manuscript reflect cumulative quantities.

Preparation of LUVs

Lipid stock of PC(16:0/18:1), PC(18:1/18:1), PC(16:0/18:2), PC(18:2/18:2) and oxidized lipids, including PC(16:0/9:0<CHO@C9>) and PC(16:0/9:0<COOH@C9>) solutions were prepared in chloroform. A certain amount of each lipid stock solution was transferred to glass tubes and dried under N_2 stream at room temperature. The solvent was further evaporated by placing the sample in a vacuum desiccator for at least 1 hour. The so formed lipid film was hydrated with 400 mM KCl solution above transition temperature of each individual lipid for around 30 minutes. The lipid suspension was then freeze-thawed

for at least 10 cycles in dry ice (mixed with ethanol) and a warm water bath (around room temperature). Afterwards, the suspension was 10 times extruded by an Avanti Mini-Extruder with filters of 200 nm porosity (Anotop 10, Whatman, Maidstone, U.K). The formed LUVs were directly used or stored at 4 °C temporarily (maximum 2 days).

Potassium (K^+) release assay

To test permeabilization of membranes by RONS, we created LUVs that contained 400 mM of KCl in their lumen. For this purpose, the lipid film created in '*preparation of LUV*' was hydrated with 400 mM KCl solution and the formation of LUVs proceeded as described. The formed LUVs were subjected to size exclusion chromatography to remove K^+ ions outside the LUVs. Specifically, Sephadex® G-50 fine (Sigma Aldrich) gel was hydrated with 400 mM NaCl solution for 2-3 hours before being transferred onto a column of 6 ml. This column was further centrifuged for 2 minutes at 2000 g to remove the water excess and 500 µl of the LUV suspension was slowly added on the top center of the column. The column was then centrifuged at 2000 g for 2 minutes and the eluate contained the LUVs with a minimal amount of K^+ ions outside the LUVs. The concentration of phospholipids was then determined by phosphorous quantification (65, 66).

The collected LUVs were diluted in PBS buffer (Na_2HPO_4/NaH_2PO_4, 50 mM, NaCl 334.8 mM, pH=7.4), having the same osmolarity as the KCl solution inside the lumen (**Fig. S2**), to a final concentration of 0.5 mM phospholipids for CAP treatment. One milliliter of each vesicle suspension was treated with CAP for 10, 20 and 40 minutes. After treatment, 400 µl of this suspension were used to quantify the total amount of K^+ inside and outside the vesicles while another 500 µl were centrifuged with 30 kDa Amicon® Ultra-0.5 Centrifugal Filter for 20 minutes at 14,000 g to separate LUVs from the released K^+ (filtrate). The percentage of the released [K^+] in the filtrate upon the total [K^+] was then determined by atomic absorption spectroscopy (AAS).

To quantify K^+ by AAS, all samples were first dried at 160-180 °C and 100 µl of 70 % perchloric acid ($HClO_4$) was added into each sample which was further mineralized at 160-180 °C for 3 hours. Subsequently, 4.8 ml of water and 100 µl of 25 % ammonia solution were added to neutralize each sample (final volume was 5 ml). The blanks for AAS consisted of PBS buffer which was subjected to all operations described for the samples.

A calibration curve was made with stock KCl solution, and its concentration ranged from 0 to 2.5 µg/ml. To account for possible interference from $HClO_4$ and ammonia, we added the same amount of $HClO_4$ and ammonia to each concentration of the calibration curve. The concentration of potassium was determined by Analytik Jena ZEEnit 700 P AAS Atomic Absorption Spectrometer at 766.4908 nm.

To determine permeabilization kinetics, we fitted K^+-release upon time to an exponential plateau model $K^+_{release}(t) = 100 - (100 - K^+_{release}[t = 0]) * exp(-k * t)$, in which ***k*** equals the release rate (min^{-1}) and t is the treatment time. $K^+_{release}(t)$ is the percentage of K^+ at a certain timepoint t while $K^+_{release}[t = 0]$ indicates the percentage of K^+ release at *t=0*, respectively. Here, 100 indicates that the maximum possible release percentage is 100 %.

Membrane packing quantification

All LUVs were made in 400 mM KCl solution and further diluted in PBS buffer to 0.5 mM phospholipids for CAP treatment. All stock solutions of fluorescent probes were prepared in ethanol and further diluted in PBS buffer. The fluorescence intensity was measured with the CLARIOstar reader (BMG LABTECH) in 96-well plates (Nunc black).

For Laurdan staining, the final concentrations for LUV and probe were 50 µM and 250 nM respectively. The staining process was conducted at 25 °C in the dark for 20 minutes directly after CAP treatment or 20 h post incubation. The excitation wavelength was 360 nm and emission intensity was scanned from 400 nm to 600 nm. The generalized polarization (GP) value was calculated from the equation $GP=(I_{440}-I_{490})/(I_{440}+I_{490})$, where I_{440} and I_{490} indicate the fluorescence intensity at 440 nm and 490 nm, respectively (67).

For di-4-ANEPPDHQ staining, the final concentrations for LUV and probe were 50 µM and 250 nM respectively. The staining process was conducted at 25 °C in the dark for 5 minutes directly after CAP treatment or 20 h post incubation. The excitation wavelength was 488 nm and an emission scan was obtained from 520 nm to 740 nm. The generalized polarization (GP) value was calculated from the equation $GP=(I_{560}-I_{620})/(I_{560}+I_{620})$, where I_{560} and I_{620} correspond to the fluorescence intensity at 560 and 620 nm, respectively (68).

Lipid extraction

For the biochemical analysis of oxidized lipids, all samples were extracted with an improved method based on Bligh & Dyer extraction method (69). Specifically, 1 ml of each LUV suspension was transferred into glass test tubes, and 3.4 ml of Bligh & Dyer solvent mixture (chloroform/methanol/1 M HCl, v/v/v, 10:23:1) was added to each tube. All samples were vortexed for 1 minute and placed on ice for 10 minutes. One milliliter of chloroform and 1 ml HCl (1 M) were added to each sample. All samples were revortexed for 1 minute and incubated on ice for another 10 minutes. Then, all samples were centrifuged for 5 minutes at 2000 g and 4 °C. The chloroform phase of each sample was taken out and transferred into new glass tubes. One milliliter of chloroform was added to wash the remaining water/methanol phase. Samples were then vortexed, and centrifuged for 5 minutes at 2000 g and 4 °C. The first and second chloroform phases were combined and 1 ml wash buffer (50 mM Tris, 100 mM NaCl, 100 mM EDTA, pH 8.2) was added before the samples were revortexed and recentrifuged in the same conditions as before. The chloroform phase was transferred to a new glass test tube and the remaining water phase was washed again with 1 ml chloroform. Finally, both chloroform phases were combined, before adding 400 µl of isopropanol (IPA) and drying the mixture under N_2 gas at ambient temperature. Hereafter, the lipid extracts were dissolved into 500 µl of methanol and extraction efficiency was determined by phosphorous assay.

Analysis with HPLC/DAD-UV-vis/MS

A Thermo Finnigan Surveyor system was used for the analysis. A reversed phase C18 column (Gemini NX-C18 150 x 2 mm x 5 µm, 110 Å; Phenomenex), with a precolumn (Security Guard Gemini-NX

4x3mm ID; Phenomenex) was used to analyze the samples and standards at a flow rate of 200 µl/min. Two solvents were used for a gradient separation. Solvent A is 5 mM ammonium acetate in Milli-Q-H_2O: isopropanol (v/v, 75:25) at pH 5.5 and solvent B is isopropanol (HPLC grade).

HPLC was coupled to a DAD-UV-vis (Thermo Finnigan Surveyor PDA Detector) and an ESI (electrospray) ion source coupled to an ion trap analyzer (LCQ Deca XP plus LC-(ESI)-MS/DAD). This combined detection allowed us to quantify and identify certain oxidized lipids (see hydroperoxides, and lipid aldehydes and ketones).

All sample and standard vials were kept at 10 °C in the HPLC sample holder. Fifty microliter of each sample or standard, together with 50 µl methanol to fill the rest of the injection loop, was injected into the LC-MS.

Separation of lipid extracts after CAP treatment by HPLC

Hundred microliter (around 100 nmole) of each lipid extract in methanol was dried with nitrogen stream and redissolved into 200 µl acetonitrile/H_2O (v/v, 50:50) by vortexing.

The gradient of mobile phase started at 10 % of solvent B, which was held for 4 minutes. This was followed by an increase of solvent B to 25 % over 2 minutes. From 10 to 18 minutes the mobile phase was held at 40 % solvent B. In the following 2 minutes the percentage of solvent B was increased to 50 %, at which percentage it was held for 6 minutes. Hereafter the solvent B is increased to 60 % in 1.5 minutes. From 29 to 38 minutes the solvent is held at 72 % of solvent B. In the following 2 minutes, solvent B was increased to 100 % and was held at this percentage for 3 minutes. Finally, solvent B was held on 10 % from 46 to 55 minutes to saturate the column for the next analysis.

Quantification of hydroperoxides

13-HPODE ((±)13-hydroperoxy-9Z,11E-octadecadienoic acid) was used as a standard to quantify the lipid hydroperoxides formed in polyunsaturated lipid extracts. Stock 13-HPODE was kept in ethanol (stored at −80 °C), and further diluted in isopropanol to make a series concentrations ranging from 2.5 to 75 µM. The gradient of mobile phase for standards started at 10 % of solvent B, which was held for 3 minutes. From 6 to 10 minutes the mobile phase was held at 40 % solvent B. In the following 2 minutes the percentage of solvent B was increased to 100 %, at which percentage it was held for 3 minutes. From 17 to 25 minutes solvent B was held at 10 % for the next analysis.

While a UV detector at 234 nm was used to quantify the hydroperoxides derived from polyunsaturated lipids (70), mass spectrometry was used in parallel to determine their structure. The PDA detector scanned a wavelength range from 190–400 nm to discern hydroperoxides with a maximum at 234 nm from other oxidation products. Mass spectra were recorded in both the negative and positive ion mode at a range from 150–2000 m/z to identify the corresponding structures.

To quantify the total amount of hydroperoxides, FOX assay was used (71). Briefly, 200 µl of FOX reagent and 20 µl of lipid extract were mixed and incubated for around 20 minutes at room temperature.

Finally, the absorbance of all samples was measured at 580 nm and H_2O_2 was used to make a calibration curve.

Quantification of aldehydes and ketones

Valeraldehyde-2,4-DNPH was used as a standard to quantify the DNPH signal. Stock valeraldehyde-2,4-DNPH was dissolved in acetonitrile (stored at 4 °C) and was further diluted in acetonitrile/H_2O (v/v, 50:50) to make a series concentrations ranging from 0.5 to 50 µM. The gradient of mobile phase for standards started at 25 % of solvent B, which was held for 3 minutes. From 6 to 10 minutes the mobile phase was held at 40 % solvent B. In the following 2 minutes the percentage of solvent B was increased to 100 %, at which percentage it was held for 3 minutes. From 17 to 25 minutes solvent B was held at 25 % for the next analysis.

Derivatization of aldehydes with 2,4-dinitrophenylhydrazine (DNPH) in combination with HPLC-DAD-MS was used to quantify their production. Specifically, 12 mM of stock DNPH reagent was made by dissolving DNPH in acetonitrile in presence of 2 % formic acid (72). Hundred microliters of lipid extract (around 100 nmole) were dried under N_2 stream before 100 µl of stock DNPH reagent and 100 µl of water were added. All samples were rigorously vortexed and kept at room temperature in the dark for 2 hours. Hereafter the samples were transferred to autosampler vials for LC-MS analysis. Valeraldehyde-2,4-DNPH (Sigma Aldrich) was used as standard to make a calibration. Limit of detection (LOD) and limit of quantification (LOQ) were determined by the standard curve (**Table S2**). We derivatized a known amount of 16:0-9:0 (ALDO) PC (1-palmitoyl-2-(9'-oxo-nonanoyl)-sn-glycero-3-phosphocholine) to evaluate the reaction efficiency. Combining mass detection (m/z) and UV absorbance at 364 nm permitted to identify and quantify derivatized lipid aldehydes.

Quantification of lipid carboxylic acids

Derivatization of carboxylic acids was done with 4-(*N*,*N*-Dimethylaminosulfonyl)-7-(2-aminoethylamino)-2,1,3-benzoxadiazole (DBD-ED) in presence of triphenylphosphine (TPP) and 2,2'-dipyridyl disulfide (DPDS) to quantify their amount in treated samples (73). Specifically, stock solutions of 5 mM DBD-ED, 28 mM TPP and 28 mM DPDS were prepared in acetonitrile. Hundred microliters of lipid extract (around 100 nmole) were firstly dried and then redissolved in 50 µl isopropanol (IPA) into which 50 µl of each stock solution (DBD-ED, TPP and DPDS) was added. All samples were vigorously vortexed and incubated for 2 hours in the dark at room temperature. Afterwards, 10 µl of each sample together with the standards were spotted on a normal phase silica TLC plate using the CAMAG® Linomat 5 (CAMAG, Wilmington, NC, USA). As external standard we used 1-palmitoyl-2-azelaoyl-sn-glycero-3-phosphocholine (PC(16:0/9:0<COOH@C9>), PAzePC, from Avanti Polar Lipids) which was derivatized in the same conditions to make a calibration curve from 0.025 to 0.75 nmole. The mobile phase to develop the TLC plate was a mixture of chloroform/methanol/water/25 % ammonia (v/v/v/v, 30:20:2:1). The image of the TLC plate was scanned with the GelDoc Go Imaging System (Bio-Rad) UV tray using the program for SYBR® Green stain. Limit of detection (LOD) and limit of quantification (LOQ) were determined by the standard curve (**Table S2**).

Semi-quantitative determination of oxidized lipids with various oxygen atoms

In addition to the fully quantitative analyses described above, we used a semi-quantitative method to determine oxidized lipids with different numbers of oxygen atoms such as hydroxyls or ketones. A full quantitative approach of these substances is difficult because of missing standards for the huge variety of oxidized lipids. The relative amount of oxidized lipids was expressed as the percentage of the corresponding peak area upon the peak area of the original lipid (corresponding host lipid that was not oxidized in the same sample). MS analysis was done in the negative ionization mode (74). We used the LPPtiger nomenclature in this manuscript and especially the supplemental material to avoid confusion of oxidized species (75).

Surface tension determination with pendant drop tensiometry

Surface tension of PBS buffer with or without LUVs was determined. For PBS with LUVs, all LUVs were made in 400 mM KCl solution and further diluted in PBS buffer to a final concentration at 0.5 mM before being treated by CAP for 40 min. LUVs without any treatment were used as negative controls. The positive controls were made by adding 0.1 % Triton-X100 to the LUV suspension. For PBS without LUVs, PBS buffer alone was treated with CAP for 40 min. PBS buffer without any treatment was used as PBS control. Positive control was obtained by adding 0.1 % Triton-X100 to PBS buffer. Surface tension of direct effects was determined directly after treatment, and 20 h post-incubation effects indicated the surface tension was determined after 20 h (at room temperature) after being treated by 40 min CAP or 0.1 % Triton-X100.

Measurements of interfacial tension between air and liquid were carried out using a pendant drop tensiometer (DataPhysics OCA) by fitting the droplet shape with the Young–Laplace equation. The liquid drop was dispensed with a 1 ml syringe together with an OKI TE needle 20 GA (METCAL).

Dynamic light scattering (DLS) analysis

LUV sizes and distribution were analyzed by dynamic light scattering (DLS) with a Malvern Zetasizer Nano-ZS at an angle of 173° for backscattering detection. All measurements were conducted at 25 °C.

Statistical analysis and principal component analysis (PCA)

Statistical analyses were performed using GraphPad Prism version 9.3.1. Data was obtained from at least two independent experiments (n=2) and multiple repeats unless stated. The comparative statistical analysis between conditions were carried out using One-way ANOVA and Two-way ANOVA comparison tests. Principal component analysis was done in Rstudio (2022.07.01, build 554) with R (v. 4.2.1.) using the ggbiplot plugin.

Supplemental information

Supplemental information includes six figures, two tables and four excel files.

Authors contributions

M.X. and E.H.W.K did the experimental work. M.X., C.A.v.W., A.S., A.F.P.S., E.B., J.A.K. and J.H.L. were involved in the conception of the study. All authors were involved in the design of the manuscript.

Declaration of Interests statement

The authors declare no competing interests.

Acknowledgements

We are grateful to Stephan A. Jonker for assisting us in the use of the AAS machine operation, Bonny W. M. Kuipers for support in DLS analysis and Martin F. Haase as well as Mohd Azeem Khan for providing pendant drop tensiometry equipment. We further thank the Alliance of financing this project. We further are thankful for suggestions and comments provided by Martijn C. Koorengevel. Min Xie was supported by a scholarship from the China Scholarship Council (CSC), https://www.csc.edu.cn/, file no. 201809370077.

References

1. Chan, H.W.S., D.T. Coxon, K.E. Peers, and K.R. Price. 1982. Oxidative reactions of unsaturated lipids. *Food Chem*. 9:21–34.

2. Vona, R., L. Pallotta, M. Cappelletti, C. Severi, and P. Matarrese. 2021. The impact of oxidative stress in human pathology: Focus on gastrointestinal disorders. *Antioxidants*. 10:1–26.

3. Sultana, S., A. Foti, and J.U. Dahl. 2020. Bacterial defense systems against the neutrophilic oxidant hypochlorous acid. *Infect Immun*. 88.

4. Brun, P., P. Brun, M. Vono, P. Venier, E. Tarricone, V. Deligianni, E. Martines, M. Zuin, S. Spagnolo, R. Cavazzana, R. Cardin, I. Castagliuolo, A.L. Valerio, and A. Leonardi. 2012. Disinfection of ocular cells and tissues by atmospheric-pressure cold plasma. *PLoS One*. 7:e33245.

5. Babington, P., K. Rajjoub, J. Canady, A. Siu, M. Keidar, and J.H. Sherman. 2015. Use of cold atmospheric plasma in the treatment of cancer. *Biointerphases*. 10:029403.

6. Laroussi, M., D.A. Mendis, and M. Rosenberg. 2003. Plasma interaction with microbes. *New J Phys*. 5:41.

7. Ytzhak, S., H. Weitman, and B. Ehrenberg. 2013. The Effect of Lipid Composition on the Permeability of Fluorescent Markers from Photosensitized Membranes. *Photochem Photobiol*. 89:619–624.

8. van Meer, G., D.R. Voelker, and G.W. Feigenson. 2008. Membrane lipids: where they are and how they behave. *Nature Reviews Molecular Cell Biology 2008 9:2*. 9:112–124.

9. Keweloh, H., and H.J. Heipieper. 1996. Trans unsaturated fatty acids in bacteria. *Lipids*. 31:129–137.

10. Lorent, J.H., and I. Levental. 2019. Preparation and properties of giant plasma membrane vesicles and giant unilamellar vesicles from natural membranes. *The Giant Vesicle Book*. 21–36.

11. Clemens, M.R., and H.D. Waller. 1987. Lipid peroxidation in erythrocytes. *Chem Phys Lipids*. 45:251–268.

12. Ytzhak, S., and B. Ehrenberg. 2014. The effect of photodynamic action on leakage of ions through liposomal membranes that contain oxidatively modified lipids. *Photochem Photobiol*. 90:796–800.

13. Boonnoy, P., V. Jarerattanachat, M. Karttunen, and J. Wong-Ekkabut. 2015. Bilayer Deformation, Pores, and Micellation Induced by Oxidized Lipids. *J Phys Chem Lett*. 6:4884–4888.

14. Bour, A., S.G. Kruglik, M. Chabanon, P. Rangamani, N. Puff, and S. Bonneau. 2019. Lipid Unsaturation Properties Govern the Sensitivity of Membranes to Photoinduced Oxidative Stress. *Biophys J*. 116:910–920.

15. Bacellar, I.O.O.L., M.C. Oliveira, L.S. Dantas, E.B. Costa, H.C. Junqueira, W.K. Martins, A.M. Durantini, G. Cosa, P. di Mascio, M. Wainwright, R. Miotto, R.M. Cordeiro, S. Miyamoto, and M.S. Baptista. 2018. Photosensitized Membrane Permeabilization Requires Contact-Dependent Reactions between Photosensitizer and Lipids. *J Am Chem Soc*. 140:9606–9615.

16. Tsubone, T.M., M.S. Baptista, and R. Itri. 2019. Understanding membrane remodelling initiated by photosensitized lipid oxidation. *Biophys Chem*. 254:106263.

17. Tsubone, T.M., H.C. Junqueira, M.S. Baptista, and R. Itri. 2019. Contrasting roles of oxidized lipids in modulating membrane microdomains. *Biochim Biophys Acta Biomembr*. 1861:660–669.

18. Schmidt-Bleker, A., J. Winter, A. Bösel, S. Reuter, and K.-D. Weltmann. 2015. On the plasma chemistry of a cold atmospheric argon plasma jet with shielding gas device. *Plasma Sources Sci Technol*. 25:015005.

19. Kowey, P.R. 2002. The Role of Potassium BT - Women's Health and Menopause: New Strategies — Improved Quality of Life. In: Lobo RA, PG Crosignani, R Paoletti, F Bruschi, editors. . Boston, MA: Springer US. pp. 151–157.

20. Volkmar, N., C.M. Gawden-Bone, J.C. Williamson, J. Nixon-Abell, J.A. West, P.H.S. George-Hyslop, A. Kaser, and P.J. Lehner. 2022. Regulation of membrane fluidity by RNF145-triggered degradation of the lipid hydrolase ADIPOR2. *EMBO J*. 41:e110777.

21. Ackerman, D., S. Tumanov, B. Qiu, E. Michalopoulou, M. Spata, A. Azzam, H. Xie, M.C. Simon, and J.J. Kamphorst. 2018. Triglycerides Promote Lipid Homeostasis during Hypoxic Stress by Balancing Fatty Acid Saturation. *Cell Rep*. 24:2596-2605.e5.

22. Kaiser, H.J., D. Lingwood, I. Levental, J.L. Sampaio, L. Kalvodova, L. Rajendran, and K. Simons. 2009. Order of lipid phases in model and plasma membranes. *Proc Natl Acad Sci U S A*. 106:16645–16650.

23. Mukherjee, S., and A. Chattopadhyay. 2005. Monitoring the organization and dynamics of bovine hippocampal membranes utilizing Laurdan generalized polarization. *Biochim Biophys Acta Biomembr*. 1714:43–55.

24. Lorent, J.H., K.R. Levental, L. Ganesan, G. Rivera-Longsworth, E. Sezgin, M.D. Doktorova, E. Lyman, I. Levental, and L.I. Lorent JH, Levental KR, Ganesan L, Rivera-Longsworth G, Sezgin E, Doktorova MD, Lyman E. 2020. Plasma membranes are asymmetric in lipid unsaturation, packing and protein shape. *Nat Chem Biol*.

25. Suhaj, A., D. Gowland, N. Bonini, D.M. Owen, and C.D. Lorenz. 2020. Laurdan and Di-4-ANEPPDHQ influence the properties of lipid membranes: A classical molecular dynamics and fluorescence study. *Journal of Physical Chemistry B*. 124:11419–11430.

26. Bacalum, M., B. Zorila, and M. Radu. 2013. Fluorescence spectra decomposition by asymmetric functions: Laurdan spectrum revisited. *Anal Biochem*. 440:123–129.

27. Jurkiewicz, P., L. Cwiklik, P. Jungwirth, and M. Hof. 2012. Lipid hydration and mobility: An interplay between fluorescence solvent relaxation experiments and molecular dynamics simulations. *Biochimie*. 94:26–32.

28. DeLong, J.M., R.K. Prange, D.M. Hodges, C.F. Forney, M.C. Bishop, and M. Quilliam. 2002. Using a modified ferrous oxidation-xylenol orange (FOX) assay for detection of lipid hydroperoxides in plant tissue. *J Agric Food Chem*. 50:248–254.

29. Navas, J.A., A. Tres, R. Codony, J. Boatella, R. Bou, and F. Guardiola. 2004. Modified ferrous oxidation-xylenol orange method to determine lipid hydroperoxides in fried snacks. *European Journal of Lipid Science and Technology*. 106:688–696.

30. Kumari, P., R.P. Singh, A.J. Bijo, C.R.K. Reddy, and B. Jha. 2012. Estimation of Lipid Hydroperoxide Levels in Tropical Marine Macroalgae. *J Phycol*. 48:1362–1373.

31. Spickett, C.M. 2014. The lipid peroxidation product 4-hydroxy-2-nonenal : Advances in chemistry and analysis Redox Biology The lipid peroxidation product 4-hydroxy-2-nonenal : Advances in chemistry and analysis $. .

32. Sousa, B.C., A.R. Pitt, and C.M. Spickett. 2017. Chemistry and analysis of HNE and other prominent carbonyl-containing lipid oxidation compounds. *Free Radic Biol Med*. 111:294–308.

33. Andreoli, R., P. Manini, M. Corradi, A. Mutti, and W.M.A. Niessen. 2003. Determination of patterns of biologically relevant aldehydes in exhaled breath condensate of healthy subjects by liquid chromatography/atmospheric chemical ionization tandem mass spectrometry. *Rapid Commun Mass Spectrom*. 17:637–645.

34. Scrimgeour, C. 2005. Bailey's Industrial Oil and Fat Products. Chapter 1: Chemistry of fatty acids. .

35. Xia, W., and S.M. Budge. 2017. Techniques for the Analysis of Minor Lipid Oxidation Products Derived from Triacylglycerols: Epoxides, Alcohols, and Ketones. *Compr Rev Food Sci Food Saf*. 16:735–758.

36. Domínguez, R., M. Pateiro, M. Gagaoua, F.J. Barba, W. Zhang, and J.M. Lorenzo. 2019. A comprehensive review on lipid oxidation in meat and meat products. *Antioxidants*. 8:1–31.

37. Ellis, S.R., H.T. Pham, M. In Het Panhuis, A.J. Trevitt, T.W. Mitchell, and S.J. Blanksby. 2017. Radical Generation from the Gas-Phase Activation of Ionized Lipid Ozonides. *J Am Soc Mass Spectrom*. 28:1345–1358.

38. Zahardis, J., and G.A. Petrucci. 2007. The oleic acid-ozone heterogeneous reaction system: Products, kinetics, secondary chemistry, and atmospheric implications of a model system - A review. *Atmos Chem Phys*. 7:1237–1274.

39. Ni, Z., B.C. Sousa, S. Colombo, C.B. Afonso, T. Melo, A.R. Pitt, C.M. Spickett, P. Domingues, M.R. Domingues, M. Fedorova, and A. Criscuolo. 2019. Evaluation of air oxidized PAPC: A multi laboratory study by LC-MS/MS. *Free Radic Biol Med*. 144:156–166.

40. Perinelli, D.R., M. Cespi, N. Lorusso, G.F. Palmieri, G. Bonacucina, and P. Blasi. 2020. Surfactant Self-Assembling and Critical Micelle Concentration: One Approach Fits All? *Langmuir*. 36:5745–5753.

41. Bai, X., L. Xu, J.Y. Tang, Y.Y. Zuo, and G. Hu. 2019. Adsorption of Phospholipids at the Air-Water Surface. *Biophys J*. 117:1224.

42. Pfeiffer, W., T.H. Henkel, E. Sackmann, W. Knoll, and W. Knoll. 1989. Local Dynamics of Lipid Bilayers Studied by Incoherent Quasi-Elastic Neutron Scattering. *Europhys Lett*. 8:201.

43. Israelachvili, J. 2011. Intermolecular and Surface Forces. *Intermolecular and Surface Forces*.

44. Reis, A., and C.M. Spickett. 2012. Chemistry of phospholipid oxidation. *Biochimica et Biophysica Acta (BBA) - Biomembranes*. 1818:2374–2387.

45. Squadrito, G.L., R.M. Uppu, R. Cueto, and W.A. Pryor. 1992. Production of the criegee ozonide during the ozonation of 1-Palmitoyl-2-oleoyl-sn-glycero-3-phosphocholine liposomes. *Lipids*. 27:955–958.

46. Bruno, G., S. Wenske, J.-W. Lackmann, M. Lalk, T. von Woedtke, and K. Wende. 2020. On the Liquid Chemistry of the Reactive Nitrogen Species Peroxynitrite and Nitrogen Dioxide Generated by Physical Plasmas. *Biomolecules 2020, Vol. 10, Page 1687*. 10:1687.

47. Reuter, S., T. Von Woedtke, and K.D. Weltmann. 2018. The kINPen - A review on physics and chemistry of the atmospheric pressure plasma jet and its applications. *J Phys D Appl Phys*. 51.

48. Nasri, Z., M. Ahmadi, J. Striesow, M. Ravandeh, T. von Woedtke, and K. Wende. 2022. Insight into the Impact of Oxidative Stress on the Barrier Properties of Lipid Bilayer Models. *Int J Mol Sci*. 23:5932.

49. Bacellar, I.O.L., and M.S. Baptista. 2019. Mechanisms of Photosensitized Lipid Oxidation and Membrane Permeabilization. *ACS Omega*. 4:21636–21646.

50. Schnitzer, E., I. Pinchuk, and D. Lichtenberg. 2007. Peroxidation of liposomal lipids. *Eur Biophys J*. 36:499–515.

51. Heuvingh, J., and S. Bonneau. 2009. Asymmetric oxidation of giant vesicles triggers curvature-associated shape transition and permeabilization. *Biophys J*. 97:2904–2912.

52. Wong-Ekkabut, J., Z. Xu, W. Triampo, I.M. Tang, D.P. Tieleman, and L. Monticelli. 2007. Effect of lipid peroxidation on the properties of lipid bilayers: a molecular dynamics study. *Biophys J*. 93:4225–4236.

53. Paez-Perez, M., A. Vyšniauskas, I. López-Duarte, E.J. Lafarge, R. López-Ríos De Castro, C.M. Marques, A.P. Schroder, P. Muller, C.D. Lorenz, N.J. Brooks, and M.K. Kuimova. 2023. Directly imaging emergence of phase separation in peroxidized lipid membranes. *Commun Chem*. 6.

54. Runas, K.A., and N. Malmstadt. 2015. Low levels of lipid oxidation radically increase the passive permeability of lipid bilayers. *Soft Matter*. 11:499–505.

55. Suhaj, A., D. Gowland, N. Bonini, D.M. Owen, and C.D. Lorenz. 2020. Laurdan and Di-4-ANEPPDHQ influence the properties of lipid membranes: A classical molecular dynamics and fluorescence study. *Journal of Physical Chemistry B*. 124:11419–11430.

56. Amaro, M., F. Reina, M. Hof, C. Eggeling, and E. Sezgin. 2017. Laurdan and Di-4-ANEPPDHQ probe different properties of the membrane. *J Phys D Appl Phys*. 50.

57. Kagan, V.E., G. Mao, F. Qu, J.P.F. Angeli, S. Doll, C.S. Croix, H.H. Dar, B. Liu, V.A. Tyurin, V.B. Ritov, A.A. Kapralov, A.A. Amoscato, J. Jiang, T. Anthonymuthu, D. Mohammadyani, Q. Yang, B. Proneth, J. Klein-Seetharaman, S. Watkins, I. Bahar, J. Greenberger, R.K. Mallampalli, B.R. Stockwell, Y.Y. Tyurina, M. Conrad, and H. Baylr. 2017. Oxidized Arachidonic/Adrenic Phosphatidylethanolamines Navigate Cells to Ferroptosis. *Nat Chem Biol*. 13:81.

58. Walker, J.E. 2013. Respiration | F-ATPases. *Encyclopedia of Biological Chemistry: Third Edition*. 2:518–523.

59. Isbary, G., G. Morfill, H.U. Schmidt, M. Georgi, K. Ramrath, J. Heinlin, S. Karrer, M. Landthaler, T. Shimizu, B. Steffes, W. Bunk, R. Monetti, J.L. Zimmermann, R. Pompl, and W. Stolz. 2010. A first prospective randomized controlled trial to decrease bacterial load using cold atmospheric argon plasma on chronic wounds in patients. *Br J Dermatol*. 163:78–82.

60. Klämpfl, T.G., G. Isbary, T. Shimizu, Y.F. Li, J.L. Zimmermann, W. Stolz, J. Schlegel, G.E. Morfill, and H.U. Schmidt. 2012. Cold atmospheric air plasma sterilization against spores and other microorganisms of clinical interest. *Appl Environ Microbiol*. 78:5077–5082.

61. Dijksteel, G.S., M.M.W. Ulrich, M. Vlig, A. Sobota, E. Middelkoop, and B.K.H.L. Boekema. 2020. Safety and bactericidal efficacy of cold atmospheric plasma generated by a flexible surface Dielectric Barrier Discharge device against Pseudomonas aeruginosa in vitro and in vivo. *Annals of Clinical Microbiology and Antimicrobials 2020 19:1*. 19:1–10.

62. Semmler, M.L., S. Bekeschus, M. Schäfer, T. Bernhardt, T. Fischer, K. Witzke, C. Seebauer, H. Rebl, E. Grambow, B. Vollmar, J.B. Nebe, H.-R. Metelmann, T. von Woedtke, S. Emmert, and L. Boeckmann. 2020. Molecular Mechanisms of the Efficacy of Cold Atmospheric Pressure Plasma (CAP) in Cancer Treatment. *Cancers (Basel)*. 12.

63. Von Woedtke, T., H.R. Metelmann, and K.D. Weltmann. 2014. Clinical Plasma Medicine: State and Perspectives of in Vivo Application of Cold Atmospheric Plasma. *Contributions to Plasma Physics*. 54:104–117.

64. Gomes, A., E. Fernandes, and J.L.F.C. Lima. 2005. Fluorescence probes used for detection of reactive oxygen species. *J Biochem Biophys Methods*. 65:45–80.

65. Rouser, G., G. Kritchevsky, C. Galli, and D. Heller. 1965. Determination of polar lipids: Quantitative column and thin-layer chromatography. *J Am Oil Chem Soc*. 42:215–227.

66. Rouser, G., S. Fleischer, and A. Yamamoto. 1970. Two dimensional thin layer chromatographic separation of polar lipids and determination of phospholipids by phosphorus analysis of spots. *Lipids*. 5:494–496.

67. Parasassi, T., G. De Stasio, A. d'Ubaldo, and E. Gratton. 1990. Phase fluctuation in phospholipid membranes revealed by Laurdan fluorescence. *Biophys J*. 57:1179–1186.

68. Jin, L., A.C. Millard, J.P. Wuskell, X. Dong, D. Wu, H.A. Clark, and L.M. Loew. 2006. Characterization and application of a new optical probe for membrane lipid domains. *Biophys J*. 90:2563–2575.

69. Bligh, E.G. and Dyer, W.J. 1959. Canadian Journal of Biochemistry and Physiology. *Can J Biochem Physiol*. 37.

70. Haefliger, O.P., and J.W. Sulzer. 2007. Rapid LC-UV-ESI-MS Method to Investigate the Industrial Preparation of Polyunsaturated Fatty Acid Hydroperoxides in Real-Time. *Chromatographia*. 65:435–442.

71. DeLong, J.M., R.K. Prange, D.M. Hodges, C.F. Forney, M.C. Bishop, and M. Quilliam. 2002. Using a modified ferrous oxidation-xylenol orange (FOX) assay for detection of lipid hydroperoxides in plant tissue. *J Agric Food Chem*. 50:248–254.

72. Andreoli, R., P. Manini, M. Corradi, A. Mutti, and W.M.A. Niessen. 2003. Determination of patterns of biologically relevant aldehydes in exhaled breath condensate of healthy subjects by liquid chromatography/atmospheric chemical ionization tandem mass spectrometry. *Rapid Commun Mass Spectrom*. 17:637–645.

73. Prados, P., T. Fukushima, T. Santa, H. Homma, M. Tsunoda, S. Al-Kindy, S. Mori, H. Yokosu, and K. Imai. 1997. 4-N,N-Dimethylaminosulfonyl-7-N-(2-aminoethyl)amino-benzofurazan as a new precolumn fluorescence derivatization reagent for carboxylic acids (fatty acids and drugs containing a carboxyl moiety) in liquid chromatography. *Anal Chim Acta*. 344:227–232.

74. Ni, Z., B.C. Sousa, S. Colombo, C.B. Afonso, T. Melo, A.R. Pitt, C.M. Spickett, P. Domingues, M.R. Domingues, M. Fedorova, and A. Criscuolo. 2019. Evaluation of air oxidized PAPC: A multi laboratory study by LC-MS/MS. *Free Radic Biol Med*. 144:156–166.

75. Ni, Z., G. Angelidou, R. Hoffmann, and M. Fedorova. 2017. LPPtiger software for lipidome-specific prediction and identification of oxidized phospholipids from LC-MS datasets. *Scientific Reports 2017 7:1*. 7:1–14.

884 **Figure Legends**

885 **Fig. 1 Plasma setup and lipids used in this study.** (**a**) The plasma source of kINPen® IND. One ml of LUV
886 suspension is treated with plasma at a distance of 2 cm to prevent that the plume touches the suspension. The
887 vector gas stream agitates the suspension evenly during treatment. Milli-Q-H_2O is added into the suspension via a
888 water pump during treatment to compensate for volume loss due to water evaporation. (**b**) Chemical structure of
889 phosphocholine lipids. 1-palmitoyl-2-oleoyl-*sn*-glycero-3-phosphocholine (PC(16:0/18:1)), 1,2-dioleoyl-*sn*-glycero-
890 3-phosphocholine (PC(18:1/18:1)), 1-palmitoyl-2-linoleoyl-*sn*-glycero-3-phosphocholine (PC(16:0/18:2)) and 1,2-
891 dilinoleoyl-*sn*-glycero-3-phosphocholine (PC(18:2/18:2)).

892

893 **Fig 2 Permeabilization kinetics, characterized via potassium (K^+) release, are drastically altered upon post-**
894 **incubation.** K^+ release in percent of LUVs made with PC(16:0/18:1) (red circles), PC(18:1/18:1) (green squares),
895 PC(16:0/18:2) (purple diamonds) and PC(18:2/18:2) (blue triangles) induced by CAP after (**a**) direct treatment and
896 (**b**) 20 h post-incubation. (**c**) Rate constant (***k***) of membrane permeabilization according to an exponential plateau
897 model described in materials and methods. One-way ANOVA analysis was used to compare ***k-values*** between
898 direct effects and 20 h post effects for all LUVs respectively. The curves represent an average from at least two
899 independent experiments done in triplicate (n≥6, *p<0.05, **p<0.01, ***p<0.001, ****p<0.0001).

900

901 **Fig 3 Laurdan (a) and di-4-ANEPPDHQ Generalized polarization (GP) (b) are altered differently upon CAP**
902 **treatment while largest changes are observed in polyunsaturated lipids upon 20h post-incubation.** Effect
903 on GP upon direct CAP treatment (dotted darker line) and 20 h post-incubation (dashed lighter line) in different
904 LUV suspensions. Two-way ANOVA analysis was used to compare the differences in GP after treatment towards
905 the corresponding negative controls. The GP values were from the average of at least two independent experiments,
906 done in triplicates (n≥6, *p<0.05, **p<0.01, ***p<0.001, ****p<0.0001).

907

908 **Fig 4 Production of oxidized products in LUVs containing lipids with different degrees of unsaturations,**
909 **induced by CAP directly after treatment (dotted line) and 20 h post-incubation (dashed line) expressed as**
910 **percentage of total phospholipids.** (**a**) Total amount of hydroperoxide functional groups, (**b**) total amount of
911 aldehyde and ketone functional groups and (**c**) total amount of carboxylic acid functional groups as a percentage
912 of total phospholipids. The total amount of hydroperoxide functional groups were determined by FOX assay (see
913 materials and methods). Two-way ANOVA analysis was used to compare the difference between CAP treated
914 samples and corresponding negative control for both direct treatment and 20 h post-incubation respectively. At
915 least two independent experiments in duplicate were performed for each assay (n≥4, *p<0.05, **p<0.01, ***p<0.001,
916 ****p<0.0001).

917

918 **Fig 5 Production and diversity of individual lipid hydroperoxides and lipid aldehydes and/or ketones**
919 **induced by CAP.** Production and diversity of lipid hydroperoxides in (**a**) PC(16:0/18:2) and (**b**) PC(18:2/18:2) LUVs
920 induced by CAP after direct treatment and 20 h post-incubation. Distribution of oxidatively truncated lipid aldehydes

and ketones (ALDO + Ketone oxbreaks), ketone oxygen addition products (ketone adducts) or DNPH signal originating from peaks that contain both type of products (unseparated) out of total DNPH signal in (**c**) PC(16:0/18:1), (**d**) PC(18:1/18:1), (**e**) PC(16:0/18:2) and (**f**) PC (18:2/18:2) directly after CAP treatment and 20 h post-incubation. The proposed structures of lipid aldehydes and ketones are presented in supplementary files (**Table S1-S4**). Two-way ANOVA analysis was used to compare the difference between CAP treated samples and corresponding negative control for both direct treatment and 20 h post-incubation respectively. At least two independent experiments were performed in duplicate for the quantification hydroperoxides, aldehydes and/or ketones (n≥4, *p<0.05, **p<0.01, ***p<0.001, ****p<0.0001).

Fig 6 Interfacial tension determination with pendant drop tensiometry. (**a**) Interfacial tension of PBS buffer containing LUVs either directly after CAP treatment or after 20 h post-incubation. 0.1 % Triton was used to make positive controls. (**b**) Proposed process of interfacial tension reduction induced by OxPCs in all above LUVs. Since PC lipids tend to form lipid bilayers, in negative control (LUV Ctrl), there are no free lipids in solution or micelles formation upon the time scale of the experiment. When a certain amount of OxPCs is formed, some OxPCs are released from lipid bilayers due to the increased hydrophilicity. Afterwards, those released OxPCs adsorb at the buffer-air interface, resulting in a reduction of surface tension. Two independent experiments were performed for interfacial tension measurements and averages are displayed in the curves.

Fig.7 PCA analysis of average membrane properties in parallel to the formation of specific OxLipids and changes of biophysical membrane properties and surface tension (brown arrows). (**a**) Untreated (red group) vs. 40 min CAP treatment (blue group), and (**b**) 40 min CAP treatment without (red group) vs. with 20 h post-incubation (blue group). Modifications of properties from individual LUV samples are highlighted by green (mono-unsaturated lipids) and purple arrows (poly-unsaturated lipids).

Fig S1 Cumulative quantities of (a) hydroxyl radicals (OH•) and (b) hydrogen peroxides (H2O2) after direct CAP treatment At least two independent experiments were performed in triplicate (n⩾6) in PBS buffer at pH 7.4.

Fig S2 CAP treatment does not influence osmolarity and pH of PBS buffer. (**a**) Osmolarity of PBS buffer (PBS Ctrl) and KCl solution before (Ctrl) and after 40 min CAP treatment (CAP 40 min) and (**b**) pH measurement after 40 min CAP. PBS Ctrl indicate PBS buffer (Na_2HPO_4/NaH_2PO_4, 50 mM, NaCl 334.8 mM, pH=7.4) without any treatment. 400 mM KCl was used to hydrate lipid films. CAP 40 min indicates PBS buffer was treated with CAP for 40 min.

Fig S3 Production of total amount of hydroperoxides as a percentage of total phospholipids via LC-MS/UV. At least two independent experiments in duplicates were performed (n≥4, ***p<0.001, ****p<0.0001).

Fig S4 Relative quantities of OxPCs expressed as arbitrary peak ratio towards the original lipid peak in LUVs made of (a) PC(16:0/18:1), (b) PC(18:1/18:1), (c) PC(16:0/18:2) and (d) PC(18:2/18:2) induced by CAP directly after treatment and 20 h post-incubation. 2×O* indicates formation of hydroperoxides and 2×O indicates formation of two 2×alcohol groups or 2 ketones. At least two independent experiments in duplicates (n≥4) were performed for semi-quantification of OxPCs.

Fig S5 Interfacial tension determination with pendant drop tensiometry. (**a**) Surface tension of PBS buffer alone induced by CAP and Triton-X 100 after direct treatment and 20 h post-incubation respectively. (**b**) Surface tension of PBS with or without addition of PC(16:0/18:1), PC(16:0/9:0<CHO@C9>) or PC(16:0/9:0<COOH@C9>) lipids from an ethanol stock solutions at indicated concentrations. Two independent experiments were performed for interfacial tension measurements.

Fig S6 DLS analysis. Intensity size distribution (%) of LUVs made with (**a**) PC(16:0/18:1), (**b**) PC(18:1/18:1), (**c**) PC(16:0/18:2) and (**d**) PC(18:2/18:2) after direct CAP treatment and 20 h post-incubation respectively. The intensity (%) size distribution indicates the relative intensity of light scattered by the LUVs in various size classes. Table shows the average size of main peak from 6 measurements and the standard derivations.

Table S1 Calculated partitioning coefficients (octanol/water, ClogP) of an original phospholipid and its oxidized counterparts. ClogP calculated by Chem Draw® Professional (version 19.1.0.8).

Table S2 Limit of detection (LOD) and limit of quantification (LOQ) of valeraldehyde-2,4-DNPH (Val-DNPH) and DBD-ED derivatized PC(16:0/9:0<COOH@C9>) (DBD-ED-COOH@C9) by LC-MS/UV and TLC analysis respectively. LOD and LOQ were calculated with GraphPad Prism version 9.3.1. based on calibration curves.

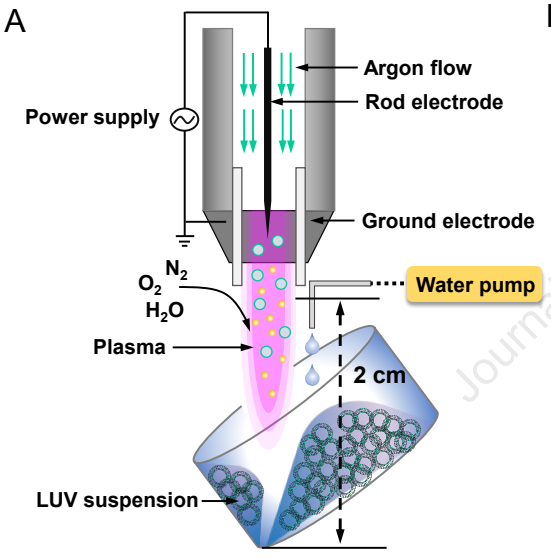

B

Asymmetric chains

PC(16:0/18:1)

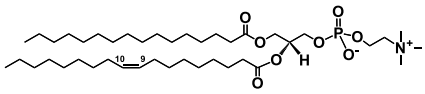

PC(16:0/18:2)

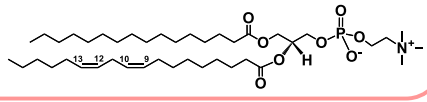

Symmetric chains

PC(18:1/18:1)

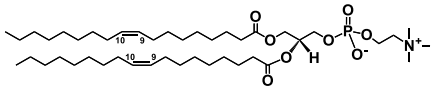

PC(18:2/18:2)

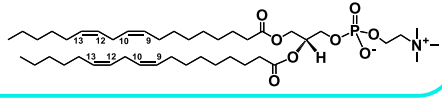

A

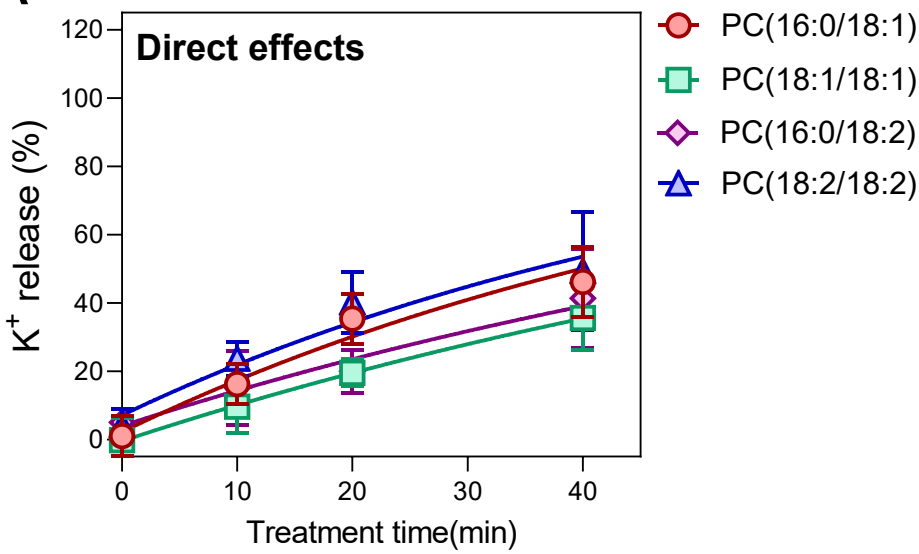

B

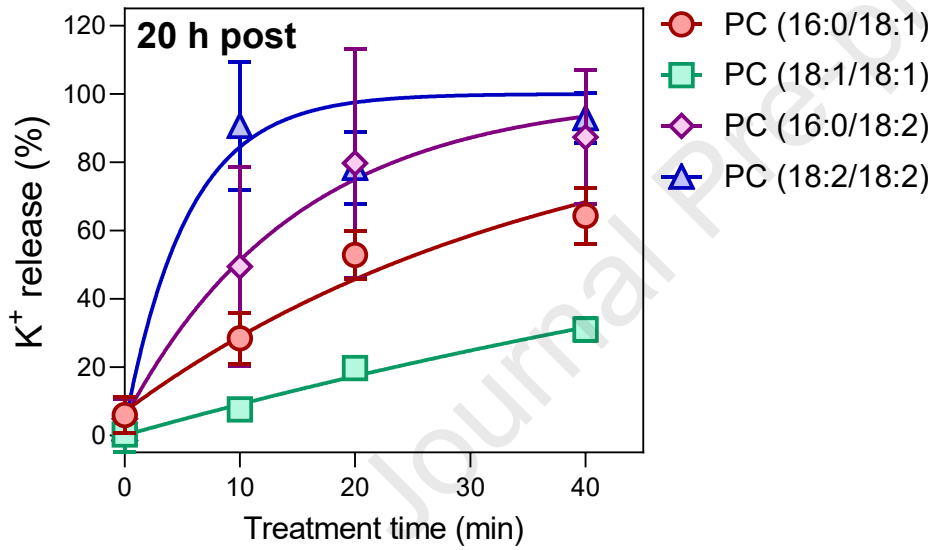

C

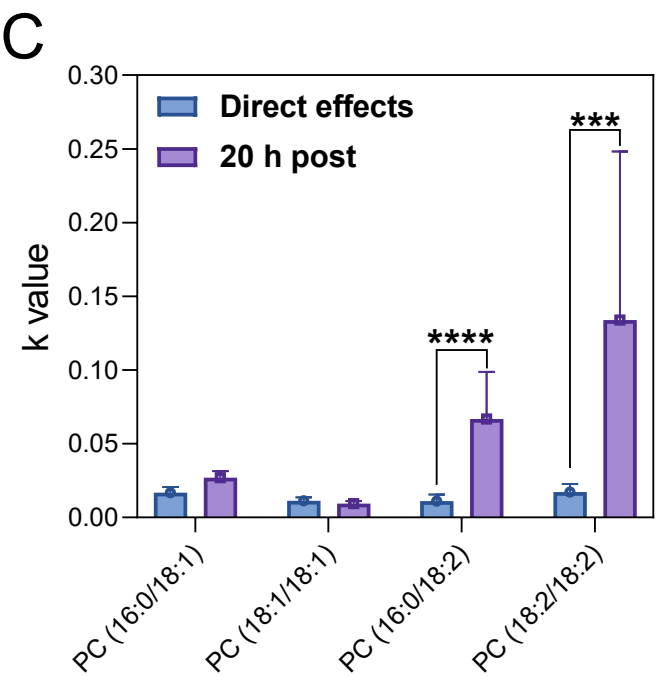

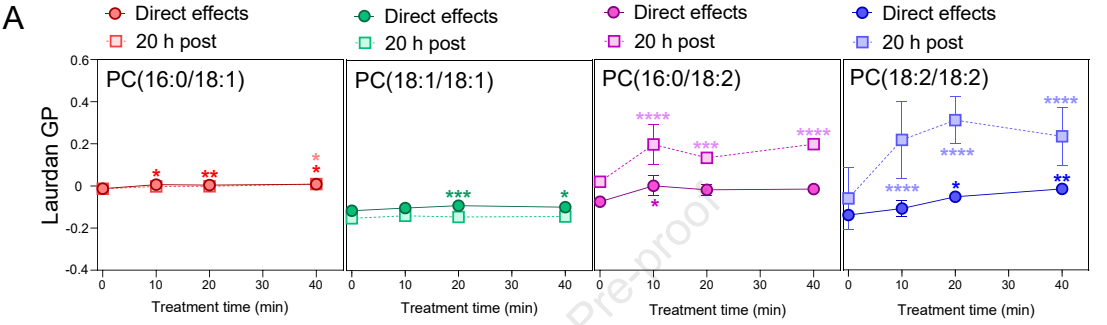

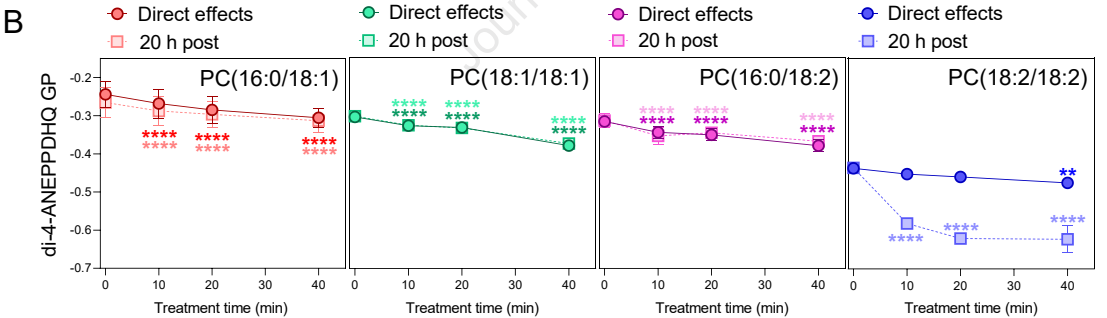

A

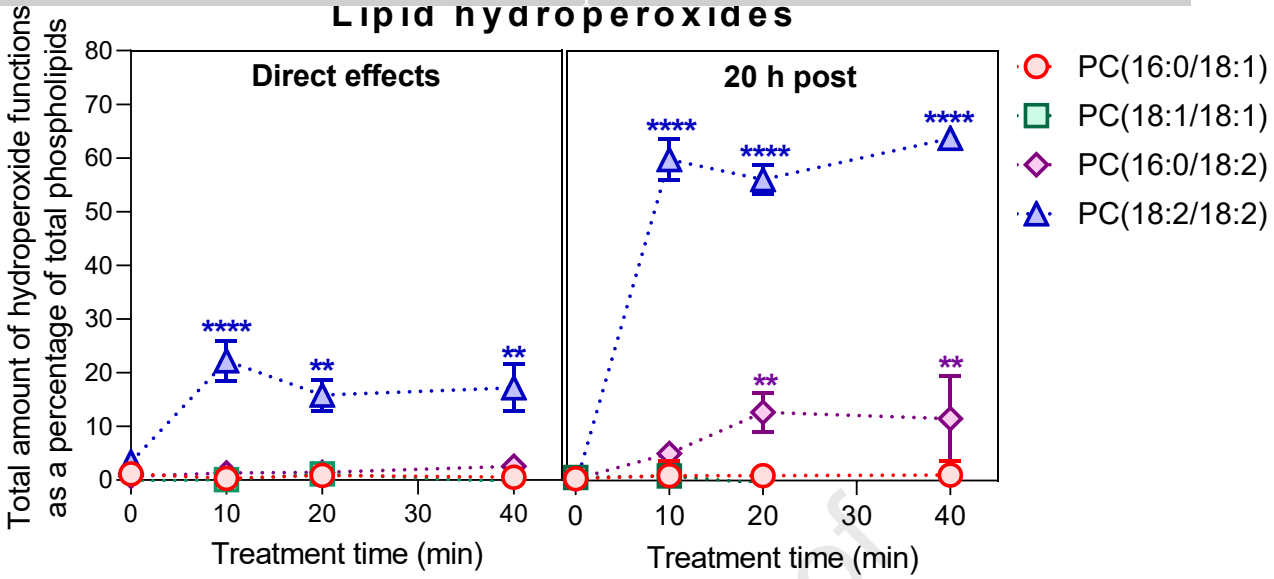

B

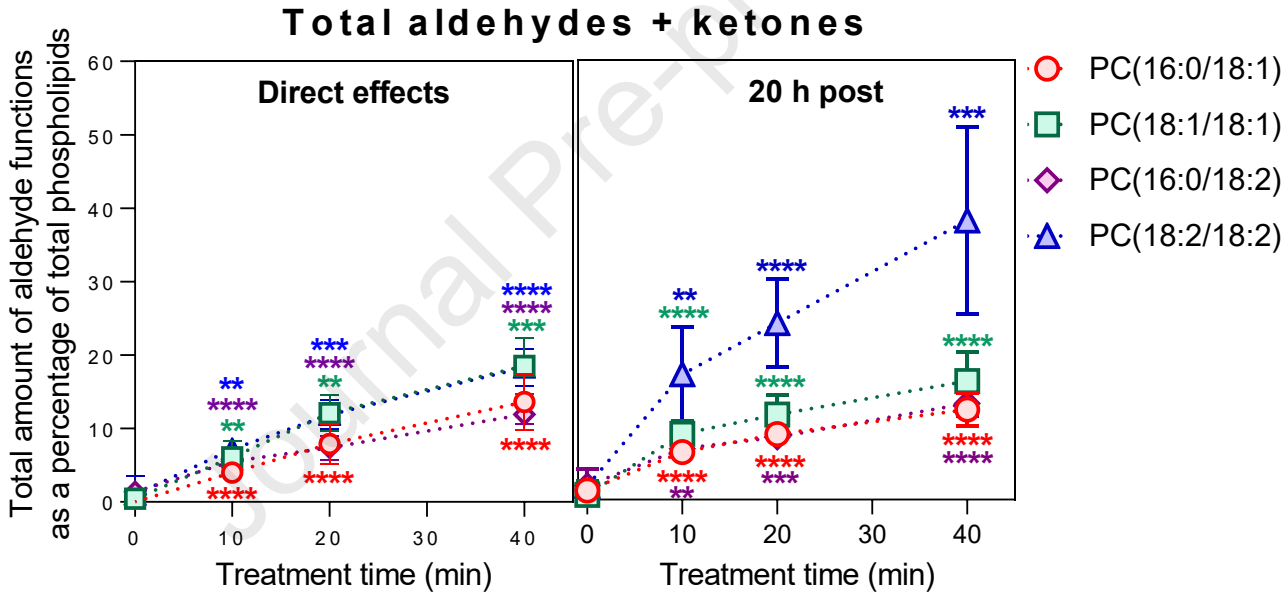

C

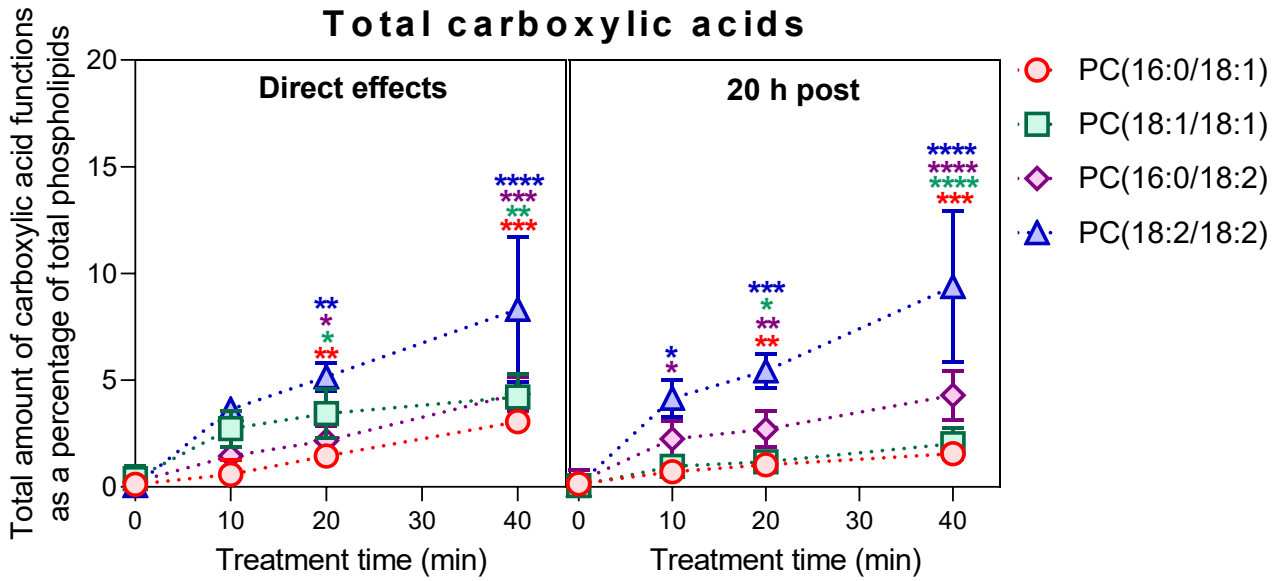

A

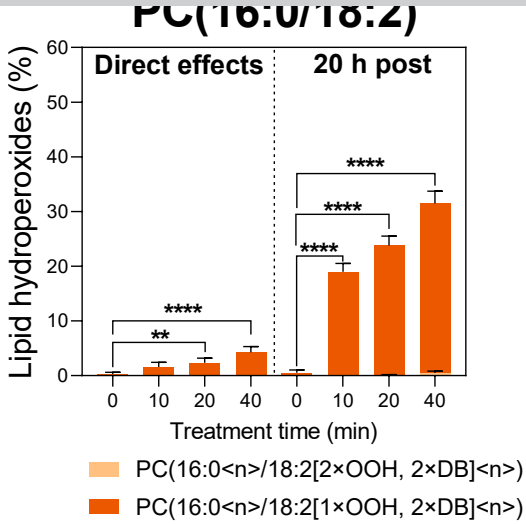

B

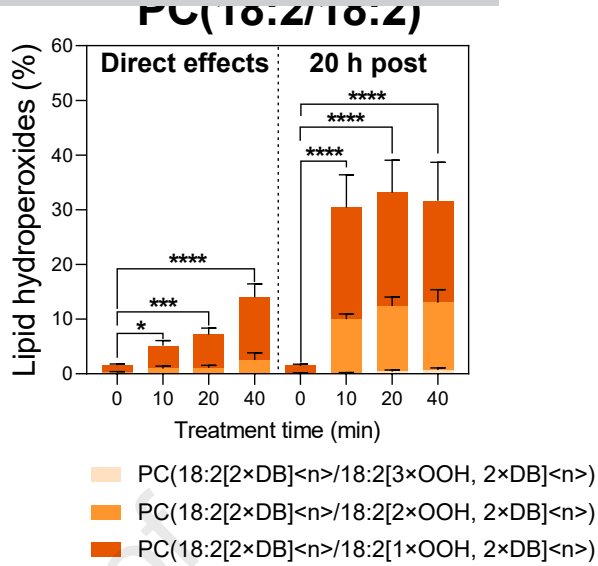

C

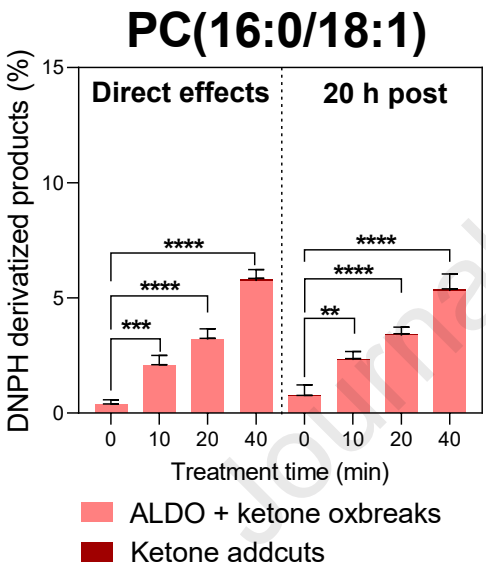

D

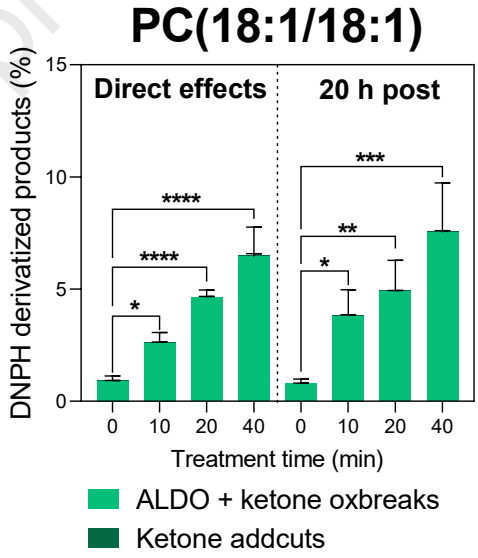

E

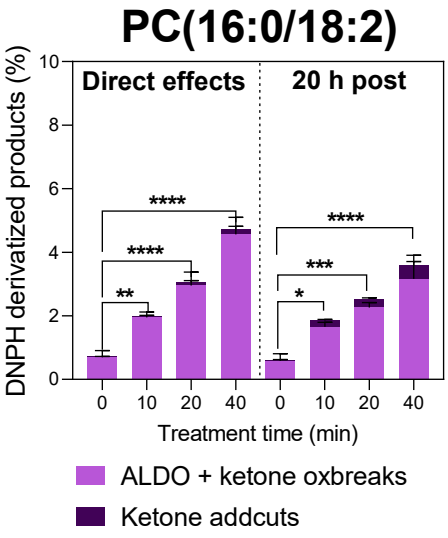

F

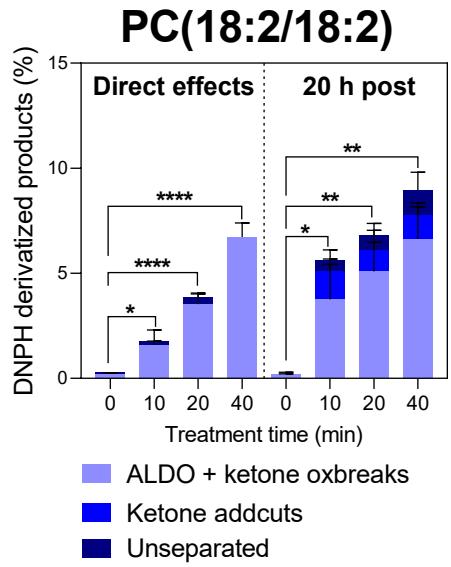

A

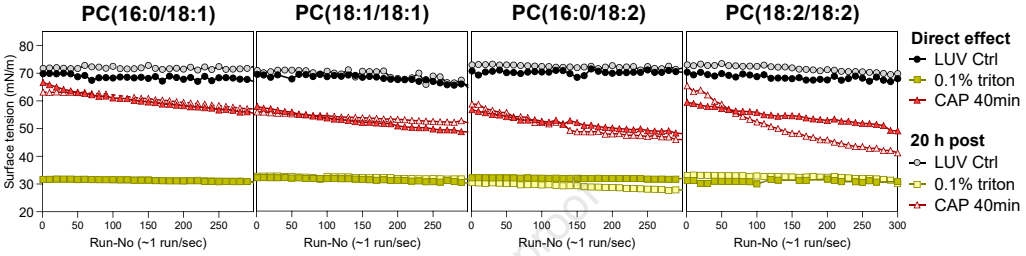

B

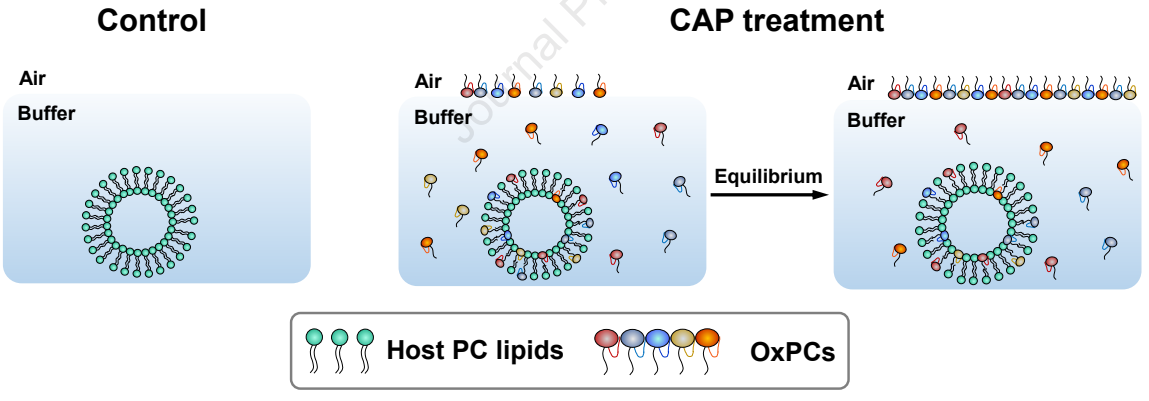

A

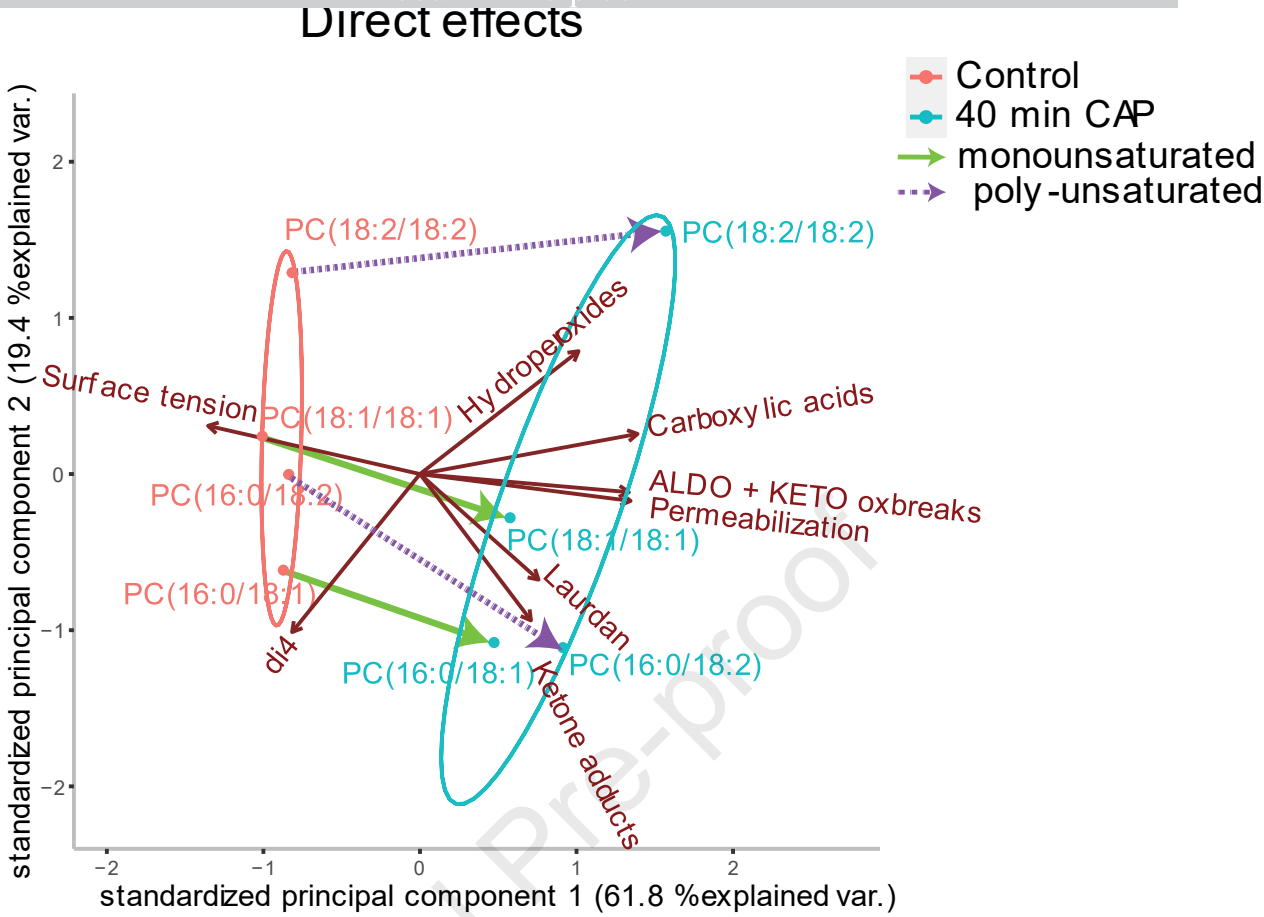

B